UNIVERSITY OF CALIFORNIA SAN DIEGO

Investigation of the Human Monomeric NEET protein MiNT

As a Drug Target in Cancer

A Thesis submitted in partial satisfaction of the requirements for the degree Master of Science

in

Chemistry

by

Maryam Ranjbar

Committee in charge:

Professor Patricia A. Jennings, Chair
Professor Joseph M. O'Connor
Professor Emmanuel A. Theodorakis

2021

The Thesis of Maryam Ranjbar is approved, and it is acceptable in quality and form for publication on microfilm and electronically.

University of California San Diego

2021

EPIGRAPH

I dedicate my success to my mother who sacrificed her life to see me at this point, to my husband who believed in me and supported me throughout the process and to my son; Arveen, who gave me strength that I never knew existed.

Table of contents

List of Abbreviations

BME	β-mercaptoethanol
cam	chloramphenicol
CBD	cluster binding domain
CIA	cluster iron sulfur cluster
CD	circular dichroism
CISD	CDGSH iron Sulfur
COPD	chronic obstructive pulmonary disease
C terminal	carboxyl terminal
DH5α	DH5-alpha cells
DM	double mutant
DNA	deoxyribonucleic acid
DNAse	deoxyribonuclease Ⅰ
DTT	dithiothreitol
E.Coli	*Escherichia coli*
ER	endoplasmic reticulum
FPLC	fast protein liquid chromatography
His-tag	histidine tag
IEX	ion exchange
IMAC	immobilized metal affinity chromatography
IPTG	isopropyl β-D-1-thiogalactopyranoside
ISC	iron sulfur cluster
kan	Kanamycin
kDa	kilodalton
LB	Luria-Bertani

LC-MS	liquid chromatography mass spectrometry
MAM	mitochondria associated membrane
MI	myocardial infarction
MiNT	mitochondrial inner NEET protein
mNT	mitoNEET
NAF-1	nutrient-deprivation autophagy factor 1
N-terminal	amino terminal
NIF	nitrogen fixation
OD	optical density
PI	isoelectric point
PMSF	phenylmethylsulphonyl fluoride
PPAR**γ**	peroxisome proliferator-activated receptor **γ**
ROS	reactive oxygen species
SDS-PAGE	sodium dodecyl sulfate-polyacrylamide gel electrophoresis
S.O.C	super optimal broth with catabolite expression
SUF	Sulfur assimilation
TZD	thiazolidinedione drug
UV-Vis	ultraviolet- visible
WT	wild type
OXPHOS	oxidative phosphorylation
GA	Gambogic acid
E-cigs	Electronic cigarettes
SCs	Schwann cells
NO	nitric oxide
AChR	acetylcholine receptor
ALS	amyotrophic lateral sclerosis
NMJ	neuromuscular junction
tSC	terminal Schwann cell
TA	Tibialis Anterior
OMM	Outer Mitochondrial Membrane

MIP	Maximum intensity projection
NMR	Nuclear Magnetic Resonance
CD	Circular dichroism
Pio	Pioglitazone Hydrochloride
DMSO	Dimethyl sulfoxide

List of Figures

List of Tables

ACKNOWLEDGEMENTS

This journey would not have been possible without the dedicated support of my family and everyone involved in my whole curriculum and experience in UCSD. I would like to thank, first and foremost, my advisor, Professor Patricia A. Jennings for giving me this opportunity for a wonderful project in NEET proteins. It is extremely difficult to find a correct fit into a laboratory especially as a master's student with limited time for research. She trusted and encouraged me throughout and this work would have not been possible without her guidance and help. Professor Jennings has helped me in many aspects in both knowledge and allowed me to experience constructive criticism in a class she taught that catered to all fields. That gave me a great experience on how realistic the world looks when presenting a research for biochemist perspective and to expect the unexpected. I am also very grateful to Professor Theodorakis and Professor O'Conner for their support and guidance with my current project and taking the time to be part of my Journey.

Working in this laboratory, I realized how crucial every member of the lab must work as one team towards the common goal in research. Together, it creates a healthy culture of a workplace that I could never hope to excerpt. I would like to thank Christopher susanto, a fellow graduate student of the similar project, for the patience to train me and help me set up an assay in Neuromuscular Junction (NMJ) project and purification of CISD3. He always willingly answered my questions even now that he does not live in the United States. He is very knowledgeable about the subject and helped me a lot in past two years. Next, I would like to thank Dr. Capraro who helped me with method modification of NEET purification and edited my thesis. Without her support in troubleshooting all kind of problems, I would have not succeeded. I am also grateful for the time she took to read my thesis and give my detail constructive feedback. I also would like to thank Grace, a fellow graduate student for the purchases she made for me for the necessary items for the experiments. I also should thank Gary

Arevalo who is graduate student in Professor Theodorakis lab and helped me with Gambogic acid binding study. He provided all different derivatives of Gambogic acid that he made so I did preliminary binding analyzes. All members of my laboratory have been very helpful and cooperative and allowed me to be very flexible with my schedule on both purification and NMJ projects.

I could not have succeeded without the help of our generous collaborator. I would like to thank Dr. Ellen Breen from the physiology department for allowing to join her lab and trusting me on study of NMJ. I also would like to thank her for letting me be part of her publication “E-cigarette vapor weakens mouse skeletal muscle force development and prevents recovery from injury”.

Outside of the department, I would like to thank my family: My mom, Azi Monro, whose tireless and loving care for my family and my boy; Arveen, over the past years has made this endeavor possible. She has supported me throughout my life and has always wanted me to be happy and do what is best for myself and I cannot give her enough thanks that she deserves. My husband, Dr. Ebrahim Amiri, who pushed me to the top and helped me to not give up and support me all these years we have been married to stay focused and do what I love in my career. Finally, my little baby, Arveen who was born in the middle of pandemic on November 15, 2020 and gave the power and strength that I never knew existed in me. Coffee did not help me to get through a day; after 2 hours of sleep at night but his love pushed me to do better. I am very grateful for all friends, family and coworkers who helped in this Journey. Without their countless love and support I would not be able to finish my work. I cannot express eternal gratitude for that other than showing them the fruits of their labor for their time and effort in me.

ABSTRACT OF THE THESIS

Investigation of the Human Monomeric NEET protein MiNT

As a Drug Target in Cancer

By

Maryam Ranjbar

Master of Science in Chemistry

University of California San Diego, 2021

Professor Patricia A. Jennings, Chair

NEET proteins belong to a class of iron–sulfur proteins that harbor a unique labile [2Fe–2S] cluster and play a major role in preventing mitochondrial dysfunction.

Loss of function in mitochondria, the key organelle responsible for cellular energy production, can result in many human pathologies including diabetes, neurodegeneration, and cancer. Despite the recent advances in molecular medicine, cancer remains a significant challenge as it is the second leading cause of death in developed countries. Therefore, additional therapies are needed to increase therapeutic options to cure diseases related to NEET proteins. Since the exciting discovery of the novel mitochondrial target, mitoNEET, for the thiazolidinedione (TZD) insulin sensitizing drug pioglitazone, the NEET family has emerged as an important class of human proteins that are implicated in multiple pathologies. There are only a few compounds that have thus far been discovered or designed as NEET ligands that control NEET [2Fe–2S] stability. The Jennings laboratory and collaborators have shown that NEET proteins act as central sensors/transducers of iron/ reactive oxygen species (ROS) metabolism were deregulation results in cell death. Specifically, recent studies have shown that small molecules can bind to NEETs destabilizing the [2Fe-2S] cluster, leading to release of iron, induction of ROS and cell death. This effect is selective for cancer cells that upregulate NEETs. These findings demonstrate, for the first time, the significance of NEETs as drug targets for a chemotherapeutic treatment of cancer.

This thesis focuses on the role of NEET proteins, specifically MiNT (CISD3), in different diseases using drug binding to examine protein stability. To further detail the unique structural difference of MiNT, as it is a monomeric protein containing two Fe-S clusters, we use a combination of biochemical and biological assays to characterize the effects of ligand binding. Specifically, we use ultraviolet visible (UV-Vis) spectroscopy and circular dichroism (CD) to monitor cluster stability over time. Together, these

assays use temperature and secondary structure analysis to determine stability effects because of ligand interactions. Given the broadened understanding of the MiNT function and the initial results from binding interactions highlighted here, it might be possible to begin the development of therapeutic agents that may be useful in mitigating several different diseases including neurodegeneration, breast cancer, diabetes, and inflammation.

Chapter 1
General Introduction

1.1 Introduction to Mitochondria

Mitochondria are membrane-bound cell organelles (mitochondrion, singular) and powerhouse of the cell as they produce most of the energy and adenosine-5′-triphosphate (ATP) required for function **(Figure 1.1)**. [1,2] Specifically, it is a cytoplasmic organelle that is essential for energy homeostasis and responsible for life and death in most eukaryotes.[2] Significantly, the mitochondria constantly undergoes a process of fusion and fission that affects its function and morphology.[3,4] Depending on the cell type, mitochondrial characteristics and function can vary. Mitochondrial dysfunction, on the other hand, is characterized by a loss of efficiency in the electron transport chain and a reduction in the synthesis of high-energy molecules, such as ATP.[5,6] Diseases that are associated with mitochondria dysfunction include neurodegenerative diseases, such as Alzheimer's disease, Parkinson's disease, Huntington's disease, and amyotrophic lateral sclerosis, Friedreich ataxia [1,3,7,8] cardiovascular diseases, such as atherosclerosis and other heart and vascular conditions [9,10]; diabetes and metabolic syndrome[10,11] autoimmune diseases, such as multiple sclerosis, and type 1 diabetes [12, 13]; neurobehavioral and psychiatric diseases, such as autism spectrum disorders, and bipolar and mood disorders [14,15];gastrointestinal disorders [16,17]; musculoskeletal diseases, such as fibromyalgia and skeletal muscle hypertrophy/atrophy[18,19]; cancer[20,21] ; and chronic infections are all associated with mitochondria dysfunction. [22,23] It is well known among researchers that mitochondrial genetic or primary mitochondrial disorders contribute to mitochondrial dysfunction and secondary or acquired degenerative disorders.[24] This process of mitochondrial ATP generation relies on oxidative phosphorylation (OXPHOS) where a by-product of this process is the generation of

reactive oxygen species (ROS). [1] Mitochondria-associated proteins are members of the NEET family which regulate iron and reactive oxygen species (ROS) homeostasis in the mitochondria.[3]

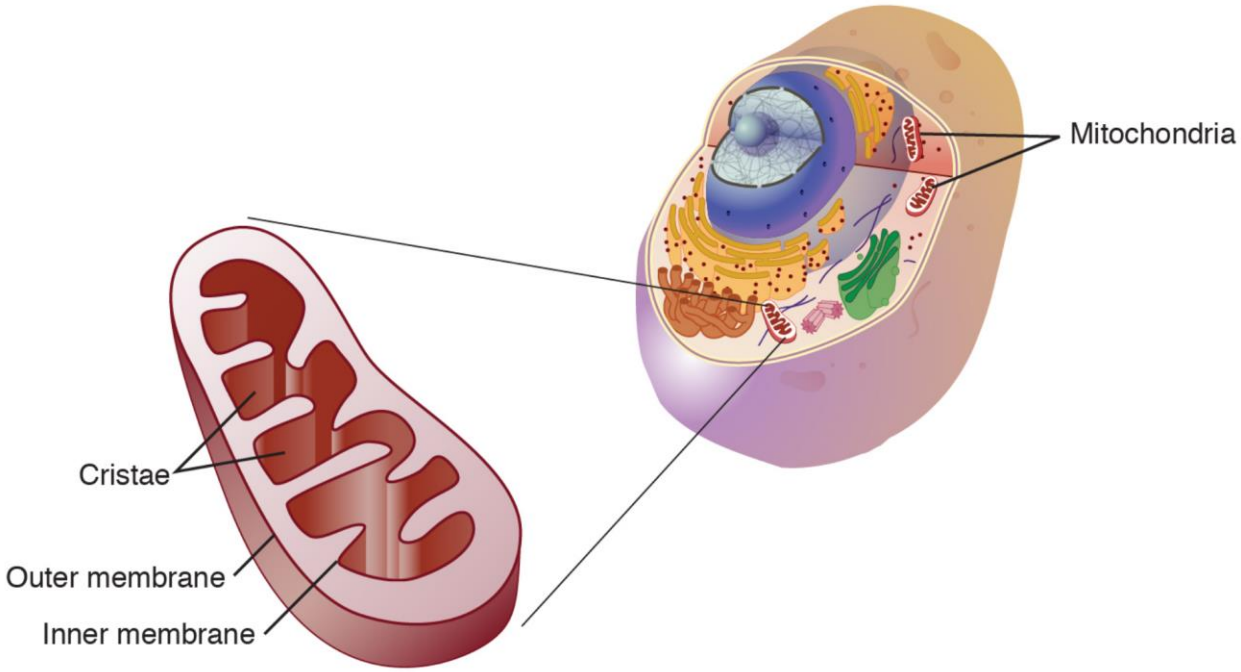

Figure 1.1: Schematic representation of mitochondria inside the cell. Mitochondria membrane-bound with two different membranes. Those membranes are essential to produce energy. That energy is produced by having chemicals within the cell go through pathways. The process of that conversion produces energy in the form of ATP, because the β, γ phosphate bond is a high-energy bond and provides energy for other reactions within the cell. Some different cells have different amounts of mitochondria because they need more energy. So, for example, the muscle has a lot of mitochondria. So, if mitochondria do not function properly, it will cause diseases and some of the diseases that mitochondrial dysfunction causes are still unknown. This figure has been adopted from Willian Gahl [1]

1.2 Iron Sulfur (Fe-S) Proteins and Cluster Biogenesis

Iron-sulfur (Fe-S) clusters are simple inorganic protein cofactors composed of ferrous (Fe^{2+}) or ferric (Fe^{3+}) iron and sulfide (S^{2-}) ions.[4] The proteins that contain non-heme iron and inorganic sulfide are present in virtually all living organisms. Additionally, they are essential cofactors for iron-sulfur clusters and are involved in numerous cellular processes such as respiration, photosynthesis, nitrogen fixation, and protein synthesis.[5,25] Indeed, iron-sulfur clusters are one of the most primitive iron cofactors known in biology [26]. Some of the common clusters that can be found in iron-sulfur proteins are from the simplest forms having a rhombic assembly [2Fe-2S] and cubed shaped [4Fe-4S], to more complex clusters having half cabane shaped [3Fe-4S]. [27] The iron ion (ferrous Fe^{2+}/ ferric Fe^{3+}) of the cluster is typically coordinated by the sulfur of a protein-bound cysteine residue or the nitrogen of a histidine residue. Iron-sulfur clusters promote electron transfer catalysis that generates redox states with a large range from +500mV to -500mV. [28] Iron-sulfur clusters are modular resulting in interconversion between different iron-sulfur proteins due to their obtainable mixed valence states. Additionally, clusters can act as biological sensors as they can react with oxygen and nitric oxide in cell development regulation.[7] In bacteria, there are three distinct pathways for iron-sulfur cluster biosynthesis: ISC, a general iron-sulfur cluster pathway, NIF, a nitrogen fixation pathway, and SUF, a sulfur assimilation pathway.[29,30] Due to the critically important roles of iron-sulfur clusters play, many organisms possess more than one iron-sulfur cluster biosynthesis pathway.[31] In human cells, there are two sets of iron-sulfur cluster synthesis: the ISC export pathway, present in the mitochondria for

cluster maturation, and the CIA pathway for cytosolic iron-sulfur clusters present outside of mitochondria (**Figure 1.2)**. [32-33]

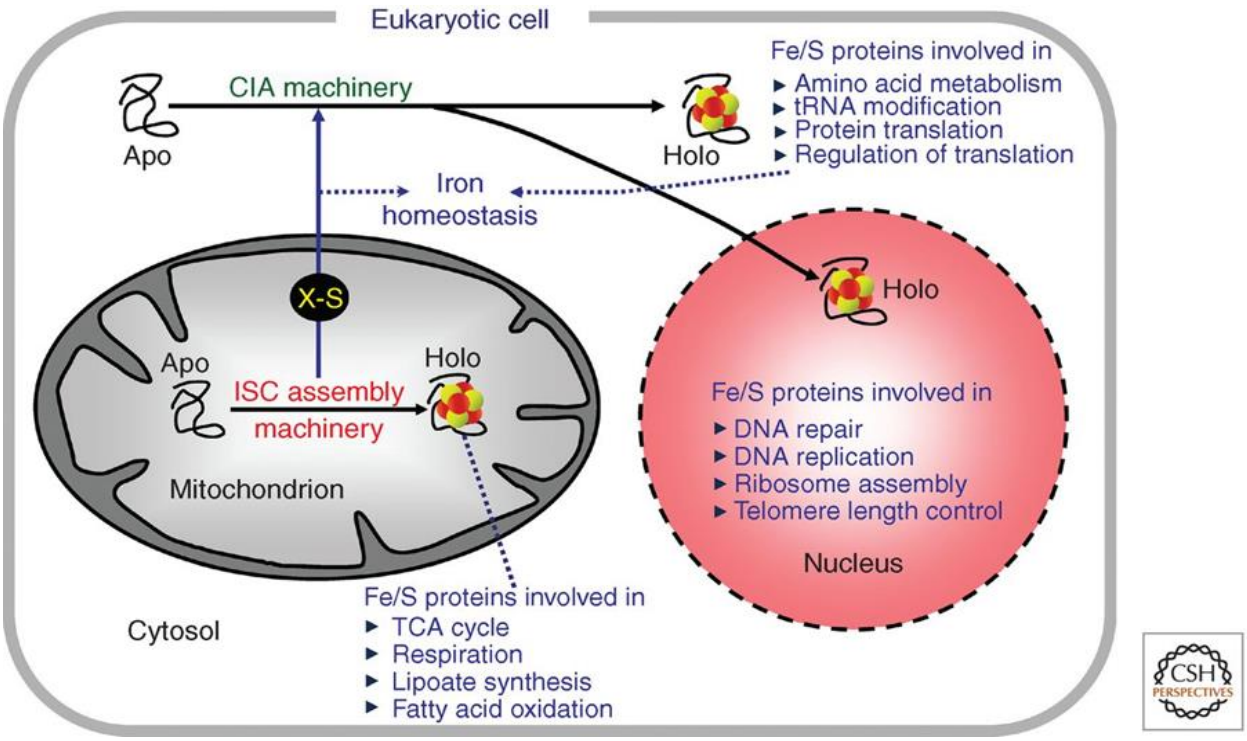

Figure 1.2: Schematic indicating the biogenesis of cellular iron-sulfur proteins in eukaryotes. Eukaryotic Fe-S proteins are in mitochondria, cytosol, and nucleus where they perform diverse functions in cellular metabolism and regulation. The mitochondrial Fe-S cluster (ISC) assembly machinery matures all organellar Fe-S proteins, and additionally contributes to the biogenesis of cytosolic and nuclear Fe-S proteins by producing an unknown sulfur-containing compound (X-S) that is exported to the cytosol and used by the cytosolic Fe-S protein assembly (CIA) machinery. Therefore, mitochondria are directly responsible for the essential functions which **link** to cellular iron homeostasis, protein translation, and nuclear genome integrity. Additionally, the ISC assembly machinery exerts a regulatory role on cellular iron homeostasis. Red and yellow circles indicate iron and sulfur ions, respectively. This figure has been adapted from Stehling, et al. [31]

1.3 Introduction to NEET Proteins

NEET proteins play a role in many human diseases such as Alzheimer's disease, diabetes, cancer, and Parkinson's disease. [34,35]These unique proteins contain two iron- sulfur (2Fe-2S) clusters coordinated by a three cysteine-one Histidine interaction, also known as CDGSH proteins, which are highly conserved from bacteria to humans.[10,15,18] In humans there are three proteins that encode the NEET family. MitoNEET (mNT) encoded by *cisd1*, *cisd2* encodes the Nutrient-deprivation Autophagy Factor-1 (NAF-1) and, *cisd3* which encodes MiNT (miner 2) (**Figure 1.3, 1.4)**. The human members of the NEET family of 2Fe-2S proteins, NAF-1mNT, are located at the interface between the mitochondria, ER and the cytosol. These proteins have been implicated in cancer cell proliferation as they can transfer their 2Fe-2S clusters to a standard apo-acceptor protein.[9]

NEET proteins are named for the Asn-Glu-Glu-Thr (NEET) sequence conserved within the sequence.[36] MitoNEET or CDSGH iron-sulfur domain 1(mNT, CISD1) localizes the outer mitochondrial membrane in humans. Nutrient-deprivation autophagy factor 1or CDGSH iron-sulfur domain 2 (NAF-1, CISD2, Miner1) is another homological human NEET protein. It primarily localizes in the endoplasmic reticulum (ER) or mitochondria associated membrane (MAM) and regulates cell autophagy. The third member of the human NEET protein is called MiNT localized inside the mitochondrial inner NEET protein. [37, 38,39]

The focus of this thesis will be on homolog in the human NEET protein family called mitochondrial inner NEET protein (MiNT, CISD3, Miner2). MiNT is an essential gene that is believed to play a role in cancer due to high expressions in human. [35]

Previous studies show that mNT (2Fe-2S) cluster mediates the oxidation of NADH by naturally reducing oxygen levels, so they are involved in electron donor/acceptor in mitochondria. [30] Computational modeling and biochemical screening has been used to identify new small molecule NEET interactions and potential drug binding sites in NEET proteins, specifically MiNT.

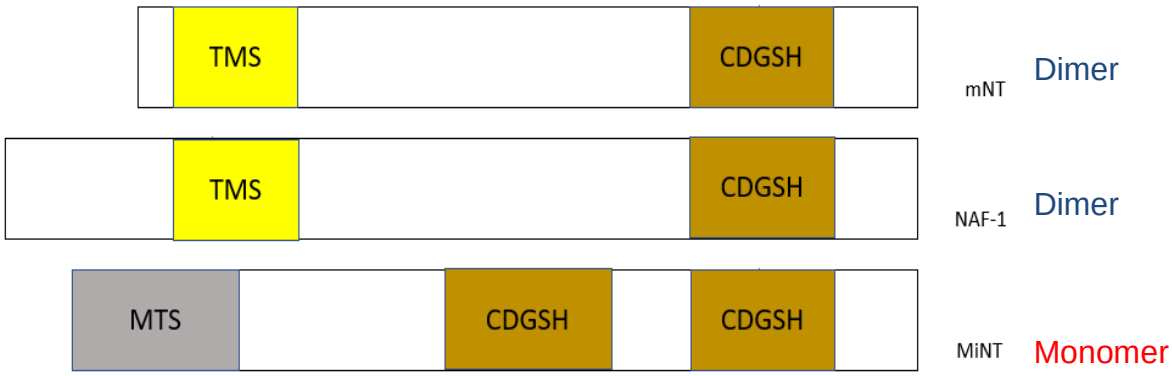

Figure 1.3: General domain alignment of three human NEET proteins. A schematic indicating the domain organization between the monomeric MiNT (bottom) versus a protomer of the dimeric mNT (top) and NAF-1(middle). Note only one of the CDGSH domains is shown. TMS refers to the transmembrane sequence and MTS refers to the mitochondrial targeting sequence of MiNT, which is cleaved upon transport into the mitochondria. Both mNT and NAF-1 are homodimers, whereas MiNT is a monomer.

Table 2.1: Amino acid sequence of MiNT (36-127) with highlighted single point mutations for each construct. Histidine and cysteines are color coordinated for clarification of differences between WT and DM.

Non-Tagged Construct of MiNT	Sequence
WT	MPARSVVALK TPIKVELVAG KTYRWCVCGR SKKQPFCDGS HFFQRTGLSP LKFKAQETRM VALCTCKATQ RPPYCDGTHR SERVQKAEVG SPL
DM	MPARSVVALK TPIKVELVAG KTYRWCVCGR SKKQPFCDGS CFFQRTGLSP LKFKAQETRM VALCTCKATQ RPPYCDGTCR SERVQKAEVG SPL

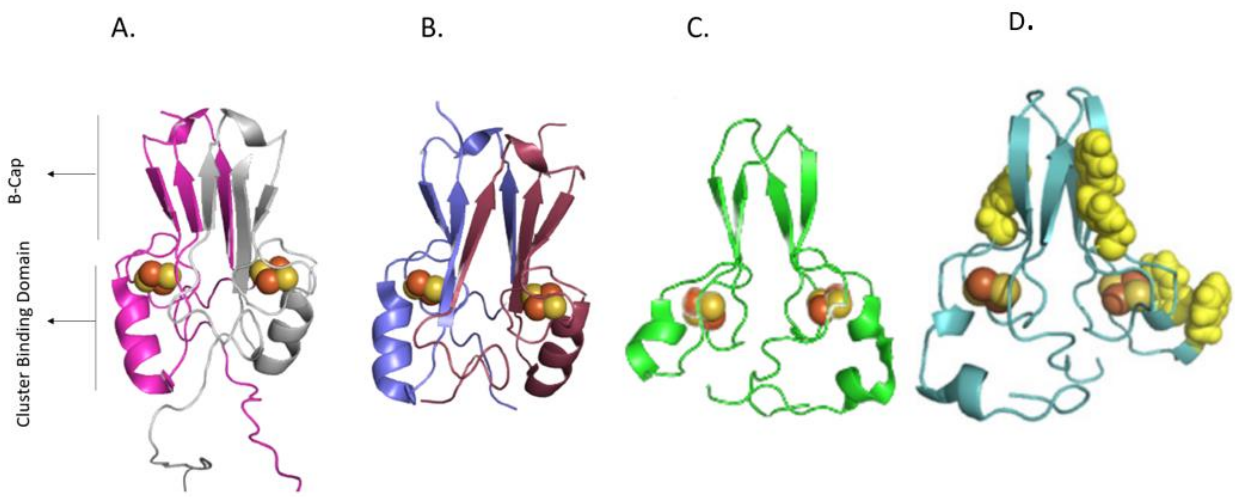

Figure 1.4: 3D representation of the crystal structures of human NEET proteins. A) mNT (PDB ID: 3EW0) the dimeric fold is colored according to the protomers, magenta and grey, respectively. B) WT NAF-1 (PDB ID 3FNV) the dimeric fold is colored according to the protomers, purple and plum, respectively. C)The monomeric cysteine mutant MiNT (PDB ID: 6AVJ) is colored green. The [2Fe-2S] cluster atoms are shown as spheres in orange and yellow. D) Structural organization of monomeric MiNT highlights the C2 pseudosymmetry and the asymmetrical surface. Ribbon diagram of MiNT with surface aromatics highlighted shows that clear asymmetry in the surface of MiNT . [35]

The human NEET proteins have all been shown to be associated with mitochondria; MiNT co-localizes with mitochondria while mNT and NAF-1 are located on the outer mitochondrial membrane (OMM). [40,41] The major parts of mNT and NAF-1 face the cytosol and a single transmembrane helix at their N-terminal region anchors each monomer of these homodimeric proteins to the OMM [42-43] NAF-1 was also found on the ER-mitochondria associated membranes (MAM) that connects the ER to the OMM, as well as to the ER [44] MiNT possesses both a beta cap and cluster binding domains, similar to mNT and NAF-1, which are signature structures in the NEET-family fold. [45] In humans, mNT and NAF-1 share about 54% identical and 69% similar residues. In contrast, human MiNT shares about 50% identical and 63% similar residues with mNT, however, it has 38% identical and 50% similar residues to NAF-1.[46] Significantly, there are sequence and structural differences. Crystal structure of the cysteine mutant MiNT indicates the domain arrangement of 2 Cluster in the CDGSH region domains (**Figure 1.4 C**) in the protomer as opposed to the homomeric mNT (**Figure 1.4 A**) and NAF-1 (**Figure 1.4 B**) containing one CDGSH domain per protomer.[12] MiNT localizes within the mitochondrial matrix, however; MiNT lacks the transmembrane domain sequence common to mitoNEET and NAF-1.While many studies of mNT and NAF-1 exist, [47] little information is available detailing MiNT function. Significantly, it has been established that MiNT is overexpressed in many cancer cells.[48] The three-Cys-one-His binding site of NEET proteins acts as a redox-sensor where the iron-sulfur cluster can be transferred to an apo-acceptor upon oxidation. In addition, all three NEET proteins are associated with the progression of diabetes, neurodegeneration, heart disease, and cancer. [7,33] An absence of MiNT can also result in an accumulation of free labile iron

and ROS, as seen in the confocal study using two different cancer cell lines suppressing MiNT expression. [37] This suggests that MiNT also regulates free labile iron, matching general characteristics of mNT and NAF-1. [7,33] Due to the overall sequence and structural asymmetry compared to the other homologs, MiNT may possess drug binding characteristics yet to be discovered that may deem it a viable and novel drug target. Thus, investigation of physical and chemical properties of MiNT is of great interest as is elucidating the functional role within iron trafficking within the ISC pathway.

1.4 Current understanding of MiNT

. MiNT is very sensitive to PH and temperature, though methods have been established that facilitate production of recombinant protein at high yields. Through purification optimization detailed in Chapter 2 and standardized assays used to determine protein stability highlighted in Chapter 3, initial details regarding MiNT are presented. Chapter 4 will highlight new preliminary data, detailing changes in MiNT biophysical characteristics upon binding to different drugs. Using sensitive optical assays such as ultraviolet visible (UV-Vis) spectroscopy and circular dichroism (CD), comparative studies will be introduced. UV-Vis spectroscopy is employed as both quantitative and qualitative assay from MiNT while CD is used to study the secondary structure changes of MiNT more carefully, as the only current structural reference to the native MiNT is through a double mutant crystal structure of MiNT. Chapter 5 will reveal a new study that is ongoing regarding Electronic Cigarettes and the effect on the body, especially on regeneration of muscles. Application of the results in the subsequent chapters will serve as a foundation for further studies by providing further insight into the function of NEET proteins.

Chapter 2
MiNT (CISD3) Methods and Modifications

2.1 Introduction

NEET proteins play a role in many human diseases including Alzheimer's, diabetes, cancer, and Parkinson's disease. [7,33] These iron-sulfur proteins are uniquely characterized by an iron-sulfur [2Fe-2S] cluster ligated to a 3Cys-1His binding domain and a beta cap domain, referred to as a CDGSH motif. The CDGSH motif is highly conserved from bacteria to humans.[11,36] There are three identified human NEET proteins: MitoNEET (mNT or CISD1), Nutrient-deprivation Autophagy Factor-1 (NAF-1 or CISD2 or Miner1) and Mitochondrial Inner NEET protein (MiNT or CISD3 or Miner2). mNT and NAF-1 have been characterized as homodimers as opposed to MiNT which is identified as a monomer.[37] mNT can be found in the outer mitochondrial membrane while NAF-1 is found primarily in the endoplasmic reticulum (ER). MiNT is found in the inner mitochondrial matrix. NEET proteins are also key regulators of iron and Reactive Oxygen Species (ROS) homeostasis, were knockdown experiments of MiNT show iron accumulation and ROS in mitochondria.[49,50] Unlike mNT and NAF-1, MiNT is not highly stable at room temperature. To purify the MiNT protein, modifications to the purification protocol in order to optimize both the yield and timeline while maintaining structural and functional integrity were necessary. In this chapter, the protocol modifications for both a Double mutant (DM) and Wild Type (WT) of MiNT protein are presented.

2.2 Transformation MiNT (CISD3) protocol

The plasmids (Pet 24a with kanamycin (kan) resistance gene in between Ndel and Xhol region) containing the double mutant from the CISD3 (2 µL) was first transformed

to 50 µl of thawed competent cells (DH5**α**) (Thermo Fisher) on ice. The reaction stood on ice for 30 minutes and then was heat shocked at 42 °C for 45 seconds. The reaction is put back on ice for 2 minutes while adding 500 µL of pre-warmed sterile Super Optimal broth with Catabolite expression (S.O.C) (Thermo Fisher Scientific) to a sterile 15 mL falcon tube. All transformation reactions are transferred into S.O.C and grown at 37 °C for one hour on a shaker at 225 rpm. It is later transferred into a 1.7 mL sterile Eppendorf tube and centrifuge at 5000 × g for 3 minutes. The supernatant is discarded leaving a pellet that contains competent cells with the incorporated plasmids. 20µL of autoclaved deionized water is added to the pellet portion in the tube where the pellet is resuspended and mixed well. Cells are pipetted onto Luria-Bertani (LB) agar plates with the appropriate antibiotics (50mg/mL of kanamycin (kan)) and grow overnight at 37 ℃.

2.3 Miniprep Purification Procedure Using Centrifuge

To isolate plasmid DNA that contained MiNT sequence of 36-127 had been previously cloned (see 2.2), we first need to purify the plasmid DNA by miniprep (Invitrogen). Most of the steps can be found as described with minor changes [51] Resuspension buffer (R3), Lysis buffer (L7) and Precipitation Buffer (N4) columns were doubled to efficiently lyse cells that results from 15mL of growth, rather than the 5 mL used in the standard protocol. Also, TE buffe volume was changed to 40 µL instead of 70 µL to get a high enough concentration of DNA for sequencing (Eton Bioscience Inc). Concentrations of the DNA were determined by using Nanodrop ND-1000 Spectrophotometer in ng/ µL at 260 nm. [52]

2.4 Expressions checks and glycerol stocks

From the isolated supercoiled plasmids (see 2.3), cells that are optimized for protein overexpression can then be used to produce the protein of interest. Here, the similar steps for transformation are taken (see 2.2), although specific BL21 (DE3) RP cells are used instead. Given the specific nature of these cells, growth media must contain both kanamycin (30 µg/mL) and chloramphenicol (30 µg/mL) (Thermo Fisher). Colonies are carefully selected, and overnights are prepared and set to grow at 37 °C in 5 mL of LB media containing kanamycin and chloramphenicol. The overnight cells are divided into two tubes containing 10 mL of LB media: containing kanamycin (kan) and chloramphenicol(cam), with each having 1:10 dilution. Here, one set is for glycerol stocks and another for an expression check. For the glycerol stock fraction, the cells are allowed to grow at 37 °C until the Optical Density (OD) reading using UV-Vis spectroscopy (Biorad SmartSpec Plus) reaches 0.5 at 600 nm. To make 1mL glycerol stocks, the cells are added to autoclaved glycerol (Thermo Fisher) at a ratio of 1:1. The glycerol stock is then stored at -80 °C. For the expression check, the cells are also allowed to grow at 37 °C until the OD600 reaches 0.8. An initial aliquot of 200 µL of cells are collected. This fraction is centrifuged at 10000 × g for 1 minute, the supernatant is discarded, and then stored in -20 °C. This fraction represents the pre-induction fraction. Next, the cells are induced, where 1mM of Isopropyl β-D-1 thiogalactopyranoside (IPTG) (Teknova) is added to the growth media. The cells are allowed to express protein at 37 ℃ for another 6 hours. After 6 hours of growth, an additional aliquot is collected and centrifuged, and the remaining cell pellet is stored in -20 °C after

removing the supernatant. This fraction is identified as a 6-hour induced fraction. SDS-PAGE gels were run to confirm the expression of the protein of interest by comparing the induced fraction 4 hour and the induced fraction 6 hour, where an increase in band intensity should be observed at the molecular weight of interest.

2.5 Results and discussion

Given the low molecular weight of the proteins of interest (i.e; DM and WT both constructs are ~ 10.2 KDa), 15% bis-acrylamide SDS-PAGE were chosen to assess protein expression and purity as it provides better resolution at the lower molecular weights, and with the available protein ladder. The recipe is as indicated below.

Table 2.2: List of reactants and volumes to generate 15% acrylamide SDS-PAGE gel.

Resolving Gel (15ml)	**Volume**	**Stacking Gel (5mL)**	**Volume**
1.5 M Tris PH 8.8	5.0 mL	0.5 M Tris PH 8.8	0.62 mL
30% acrylamide	7.5 mL	30% acrylamide	0.83 mL
Water	2.4 mL	Water	3.82 mL
20% SDS	75 µL	20% SDS	25 µL
10% APS	75 µL	10% APS	50 µL
TEMED	25 µL	TEMED	5.0 µL

For all samples, add 16µL of cell, 4 µL of 2 × Loading buffer and 1 µL

β-mercaptoethanol (BME) (Biorad). They are then heated to at least 85 ℃ for a few minutes until condensation can be seen on the tube cover, then removed to cool down to room temperature before loading into the well . Approximately, 10 µL of each sample is added to fill each individual well of the stacking gel where an additional well was left for 10 µL of G02101 Accurulaer Prestained Protein Ladder (Lamda Biotech) as molecular size comparison standard. The loaded gel(s) was run at 120 V for about 2 hours. Gels were then stained with Coomassie Blue stain for overnight and next day de-staining for band visualization. Gel results were photographed, and image files were saved. **Figure 2.1** represents a typical expression check gel.

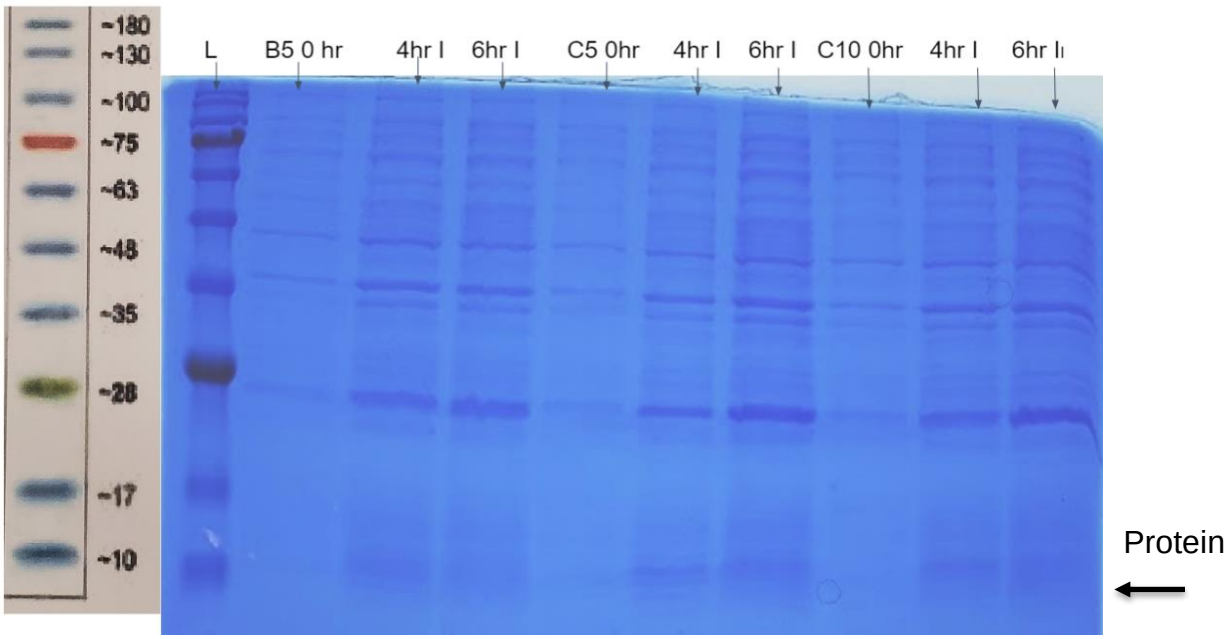

Figure 2.1: Expression Check DM CISD3: 15% SDS-PAGE indicating the pre and post induction of three different samples: B5, C5 and C10. For each sample, at 0-hour (0hr) is when OD600 reached 0.8 prior to induction. Fractions that were induced with IPTG and expression were allowed for 4 hour and monitored for an additional 6 hours (induced, I, fractions).

2.6 Growth of cells and purification of NEET proteins: NAF-1 and CISD3

2.6.1 Cell growth and expression protocol for NAF-1 and CISD3

Both NAF-1 and CISD3 proteins have similar growth protocols with the exception that CISD3 without supplemental $FeCl_3$. A 200 mL LB media starter containing 30mg/mL kan and 30mg/mL cam is used to grow the cells overnight at 37 ℃ with a rotation speed of 180 rpm. Overnight cells are then evenly aliquoted into the larger 2 L of LB media, each containing kan and cam, for growth. Once OD600 reaches 0.5, 500ml of freshly autoclaved $FeCl_3$ is added equally to each 2L of LB. For CISD3, we do not add $FeCl_3$. The growth is then allowed to continue to reach OD600 of 0.8 where induction is initiated with the addition of 1mM IPTG. cells are allowed to express for 18 hours at 18℃. After overnight growth, cells are harvested by centrifugation (Avanti Centrifuge J-20XP) with JLA-8.1000 rotor (Beckman) at 3000 rpm and 4 ℃. The supernatant is removed and 50 mL of lysis buffer containing 50 mM Tris (Sigma Life Science) pH 8.0 and 50 mM NaCl (Fisher Chemical) is added to the pellets and stored at -80 ℃. For optimal purification, the cells must store in -80 ℃ at least a day for easier shearing.

2.6.2 NAF-1 purification

Stored cell pellets are thawed at room temperature and resuspended in a sonication buffer (50mM Tris-HCl pH 8.0, 500 mM NaCl) and solution was the sonicated using 550 Sonic Dismembrator (Thermo Fisher) programmed for a 5 second pulse and 15 seconds off for a total of 10 minutes. The cell lysate is then centrifuged for 30

minutes at 13,000 rpm (JA10 rotor) using 35 mL tubes. The supernatant is added to 5-10 mL of Ni-NTA resin (Qiagen) slurry and is batch bound for 30 minutes. The mixture is then slowly poured into a column and allowed to flow through, stirring occasionally to assist in complete gravity flow. The resin is washed with 10 column volume (CV) of wash buffer 1 (50 mM tris-HCl pH 8.0, 5mM Imidazole, 300 mM NaCl) initially. Subsequently, the resin is washed with an additional 5-10 CV of wash buffer 2 (50mM Tris-HCl pH 8.0, 30 mM Imidazole, 300mM NaCl). The poly-His construct includes a thrombin cleavage site; therefore, the His-tag is cleaved using 2 mg of thrombin (Thermo Fisher) equilibrated in a thrombin cleavage buffer (25mM Tris-HCl pH8.0, 50mM NaCl, 2.5mM CaCl2) with the washed slurry for 20 hours at 4 ℃. Equilibration is achieved. The flow through is discarded and the cleaved protein of interest is eluted with a low-salt wash buffer 3 (25mM Tris- HCl pH8.0, 20 mM NaCl, 40 mM imidazole) twice using 5CV. Finally, this step is repeated but the mixture is allowed to sit for 15 minutes to maximize protein recovery.

The protein recovered at this point contains other contaminants, thus an additional cation exchange chromatography (HiTrap, GE Healthcare Biorad) step is used **Figure 3.1** and **Figure 3.2**. Using a two-buffer approach where high ionic interaction helps isolate the protein of interest based on charge, Buffer A (50 mM Tris pH 8.0) and buffer B (50 mM Tris pH 8.0, 500 mM NaCl) where used to charge and equilibrate the column. The programmed protocol included five CV of 100% buffer B followed by at least 10CV of buffer A (0% B) to be flowed through the detector. Additionally, it includes a 5CV wash with 15% buffer B and finishes with a 20-25 CV gradient from 15% to 60% buffer B, followed by 5CV of 100% buffer B to clean the

column. The protein of interest elutes around (80-90 CV). The protein is then concentrated in a 15-mL centrifugal concentrator with a 3 KDa cutoff filter to approximately 1mM. The protein purity is analyzed by 15% SDS-PAGE and UV-Vis spectroscopy, comparing the A 280 to the A 458. The extinction coefficient for NAF-1 8500 M^{-1} cm^{-1} at 280 nm and 10000 M^{-1} cm^{-1} at 458 nm. [53,54] Purified protein is then stored in -80 °C

2.6.3 CISD3 purification Original method

Original method adopted by Christopher Susanto. Frozen harvested cells of CISD3 are thawed and 1 mM of PMSF is added to the mixture. Cell pellets are diluted with up to 100 ml of lysis buffer (50mM Tris pH 8.0 ,50 mM NaCl) before using an Avestin Emulsiflex-C5 High pressure homogenizer for lysis (ATA Scientific). After homogenizing, 40 µL of Deoxyribonuclease (DNase I) (New England Biolabs) and 2mM $MgCl_2$ are added to the mixture and incubated at room temperature for 20 minutes. After incubation, the mixture is transferred to a 50 ml tube and centrifuged at 15,000 rpm and 4 °C for 45 minutes. The supernatant is collected and filtered with a 33 mm diameter 0.22 µm syringe filter unit, (Millipore) twice. The filtered supernatant is then subjected to cation exchange by FPLC, similar to NAF-1 (see 2.6.2). The supernatant is injected into the FPLC machine and purified by cation exchange in three steps using a single HP SP 5mL column (GE Healthcare Life Science). The buffering system included Buffer A (50 mM Tris pH 8.0) and Buffer B (50-mM Tris pH 8.0, 1 M NaCl), respectively. The initial cation exchange run is isocratic at an ionic concentration of 360 mM NaCl. The second and third cation exchange runs use a gradient from 30 mM NaCl to 600 mM

NaCl. The reducing agent dithiothreitol (5mM, DTT) (Biopioneer) is only added to the purification of WT CISD3 under cold conditions (Ice). The protein of interest in this method eluted around 12-15 CV (330-360mM NaCl) and resulting eluent is further purified by size exclusion chromatography using a HiPrep 26/60 Sephacryl (S-100) (GE Healthcare Life Science) for the final purification step. The buffer used to run the size exclusion column contained 50 mM Tris pH 8.0, 150mM NaCl and 5mM DTT. The protein DM elutes around (12-15CV which is 310-350mM NaCl) and WT elutes around (14-16CV which is 340-380 mM NaCl). The elution fraction is then combined and concentrated. Solution undergoes buffer exchange over several dilutions may occur to remove DTT. Comparing the A 280 to the A 458. The extinction coefficient for CISD3 8855 M^{-1} cm^{-1} at 280 nm and 10000 M^{-1} cm^{-1} at 458 nm. [55] The concentrated protein samples are flash frozen and stored at -80 ℃. [50]

2.6.4 CISD3 Purification Modifications

CISD3 constructs are sensitive to temperature over time, thus modifications to the ion-exchange steps in the protocol were explored in order to reduce the amount of time the protein is exposed to stressful conditions. We tested four slightly different methods: A, B, C and D, where modifications were made within the programming of the gradient buffer. For these respective runs, Buffer B was modified to 50mM Tris pH 8.0, 600 mM NaCl, and an additional column was added resulting in two stacked 5mL of HP SP columns (GE Healthcare Life Science).

The initial exploratory run of **Method A** included a 5CV wash with Buffer A, 0% Buffer B, followed by a wash with 10CV of 20% Buffer B, then a gradient from 20% to

45% Buffer B. These wash steps are followed by 10CV of 45%B and finally 5CV of 100% Buffer B in order to remove any remaining contaminants in the column. Fractions were collected from the various steps in the protocol and run on an SDS-PAGE gel in order to determine isolation efficacy. Protein of interest was concentrated in a 15 mL centrifugal concentrator with a 3 KDa cutoff until the protein solution was near 1mM. A second attempt, **Method B,** is similar to method A with modifications at the various gradient steps, optimizing for greater peak resolution. The volume of buffer used to column wash was increased (10CV) which accounts for the larger void volume because of the stacked columns. Furthermore, as peaks began to elute in the initial gradient jump, the isocratic flow was set to 15% for 10CV, then dropped down to zero for 5 CV in order to clear contaminants. To maximize the elution of the interest protein, a steeper gradient from 30% to 75%B was tested. From here, the isocratic flow was increased to 100% Buffer B for 10CV followed by lowering it to zero for 10CV. We expected the changes to yield the protein of interest within the steep gradient step. However, the result showed two sharp peaks and we are looking to make it work as a single sharp peak as possible. Therefore, we modified **Method B** a little further to test whether there is a mixture of holo (active form) and/or apo (inactive form) of the CISD3 DM construct **Chapter 3** that may co-elute within the same peak. In this method, the gradient is shallower on the elution step. **Method C** deviates from **Method B** with the gradient initiating at 40% Buffer B for 10CV. The shallower gradient allows the protein to elute around 55% Buffer B, where sharper and multiple peaks are present. Finally, an additional improvement from **Method C** where small alterations were made resulting in the protein eluting around 330mM NaCl and sharper and stronger peaks, **Method D**

lengthens the second elution to 10CV instead of 5CV at 0% Buffer B, allowing the column to wash more thoroughly before the steep gradient.

2.6.5 Size Exclusion Column (SEC) Chromatography

Following the cation exchange chromatography, the eluted fractions of interest are combined, concentrated, and buffer exchanged to a final volume that is approximately 10mL. The SEC column is equilibrated with 50 mM Tris pH 8.0, 150 mM NaCl. Prior to injection, 100mM of PMSF is added to the concentrated protein solution. The SEC chromatogram reveals the protein elutes at 255-285 mL. SDS-PAGE gels were used to confirm the efficiency of each step as well as the size and purity of the protein peaks. The protein concentration was assessed by comparing the UV-Vis spectrum at A 280 to A458. The peak of interest was collected and concentrated and flash frozen for immediate storage at -80 °C. Purified protein is then stored at -80°C.

2.7 Biophysical assays and analysis

Ultraviolet-Visible (UV-Vis) Spectroscopy

Stability assays of protein NEET CISD3 were carried out using a Cary 50 Bio (Varian) spectrometer connected to a CFT-25 Refrigerated recirculating water bath. Samples of protein (20 µM) were prepared in a buffer containing 50 mM Tris pH 8.0, 150 mM NaCl. Assays were performed at 37 °C, with a 1 cm pathlength quartz cuvette (Spectrocell). Additionally, l 100 µL of paraffin oil (Hampton Research) was added to the top of the sample to prevent evaporation and condensation. Each assay depends if pioglitazone (pio) or Gambogic acid (GA) was run as 20 µM of CISD3 protein, 10%

DMSO and/or 10%DMSO with a drug of interest (pio or GA). Method ran 200-800nm for 100cycle and 10 or 20 minutes/cycles. Data was analyzed using an excel sheet shown in **Chapter 4.**

Circular Dichroism (CD) Spectroscopy

Multiple experiments were conducted using a Circular Dichroism Spectrometer Model 215 (Aviv Instruments Inc). Protein was scanned in several different wavelength ranges:200 nm to 300nm and 300 nm to 800 nm. Protein samples of 20 µM in a buffer containing 50 mM Tris pH 8.0 and 150 mM NaCl were scanned in a 0.1 cm pathlength cuvette. A Peltier temperature controller was also used to maintain the individual 15 °C runs. The AVIV in-house software was used to set up collection parameters with a data pitch of 1 nm, 50 nm/min scanning speed and 1 nm bandwidth. Scans were typically averaged over three runs. The Spectra Analysis program was used to analyze the spectra. For the near to far UV-range of 200 nm to 300 nm, **Chapter 4** will show the overall structure was assessed and compared between WT and DM proteins. was collected at 15 °C and 37 °C. Samples collected from 300 nm to 800 nm assessed to analyze if the cluster is being changed when additional small molecules are added.

Chapter 3

Purification Results CISD3 Protein with New Method

3.1 Introduction

Modification of NAF-1 purification done first for comparative reason and to ensure that the structure of protein will retain, and **Figure 3.1-3.3** shows result of purification and decay. The objective of modifying the protein purification protocol CISD3 is to maximize the yields of the protein of interest while maintaining its structural and functional integrity. Purification steps of a non-tagged construct of MiNT before modification were limited. We modified the method to increase reproducibility of purified protein, less time and higher yield. Lysate is extremely viscous after homogenizing and that made harder to purify with old method, an excess amount (40 µL of 2000 U/mL stock) of bovine pancreatic deoxyribonuclease I (DNase I) with 2 mM $MgCl_2$ are added into the homogenate and it is incubated for 20 minutes at room temperature. This ensures that most of the DNA has been cleaved. Cation exchange is run only one time in the new method and that helps with yield as well as time. An example of a chromatogram is as shown below for the DM construct elution. **Graph 3.4** shows the A-D IEX method and since DM is more stable at room temperature compared to WT. We used DM to test different methods and to get better results, we used two SP HP 5mL columns in the IEX step.

3.2 Result and discussion

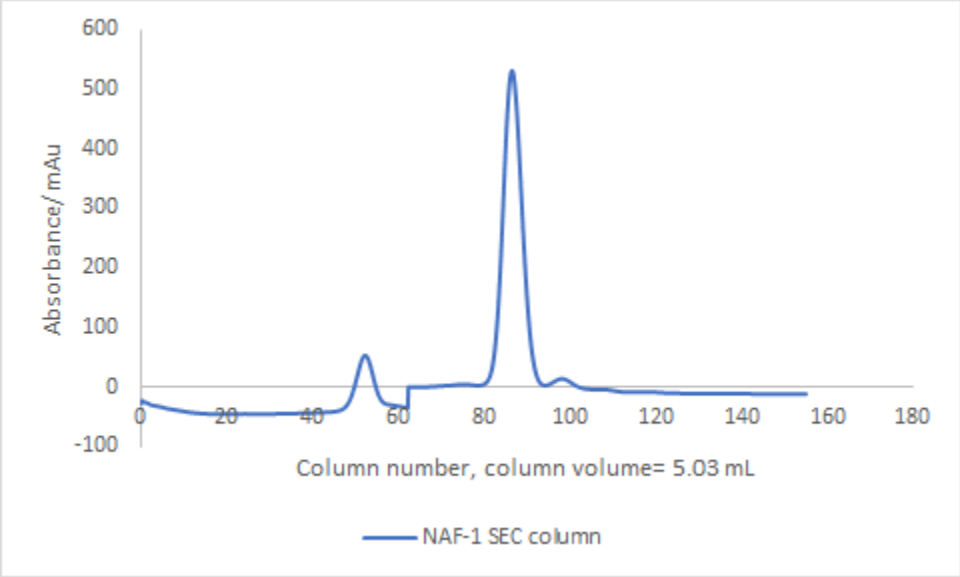

Figure 3.1: FPLC chromatogram of NAF-1 with thrombin cleaved site purification S100 column. Last step of purifying NAF-1, Size Exclusion column s100 has been used to clean protein.

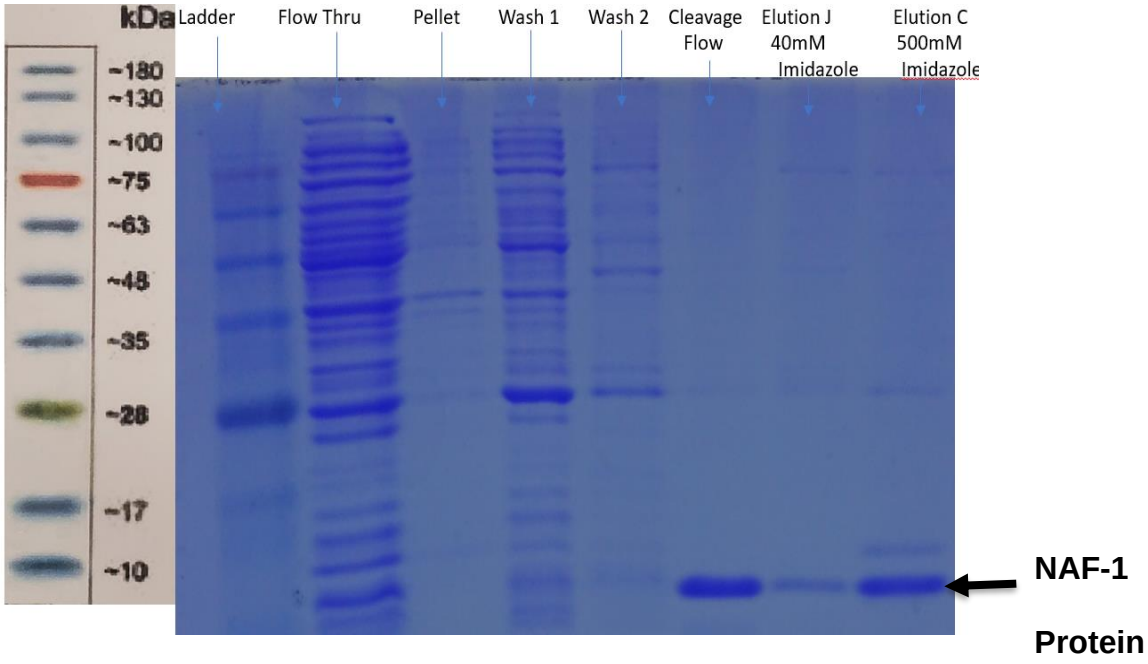

Figure 3.2: SDS Gel of NAF-1 thrombin Cleavage. This Gel shows wash 1 as 5mM imidazole, wash 2 ,35mM imidazole. Cleavage flow though; 50mM NaCl + 2.5mM CaCl2 + 25mM Tris pH 8.0. We are expecting to see protein at around ~9.6 KDa band in to make sure of purification steps .

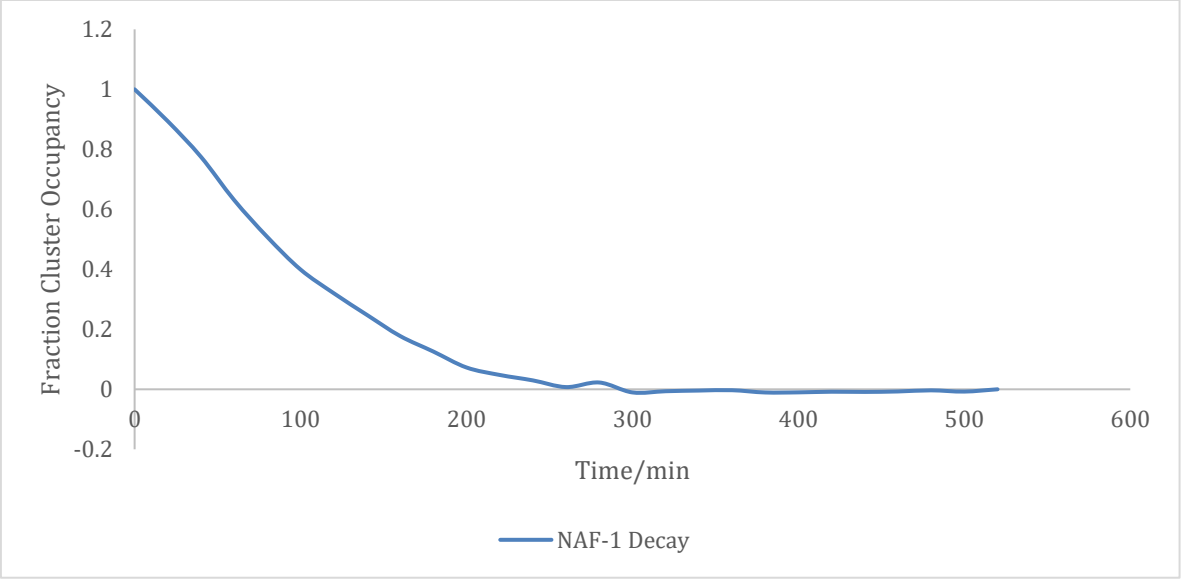

Figure 3.3: This graph shows decay NAF-1: it ran 50 cycles for 20 min/cycle. Buffer condition SEC; 50mM Tris PH 8.0 + 150mM NaCl. Half life of NAF-1 is around ~ 250 minutes.

Figure 3.1-3.3 showed modified purified NAF-1 with thrombin cleavage still retains structure and protein shows half-life of 100 minutes. Following data **Figure 3.4-3.9** shows modified purification of CISD3 protein and different methods tested to get a higher yield faster method.

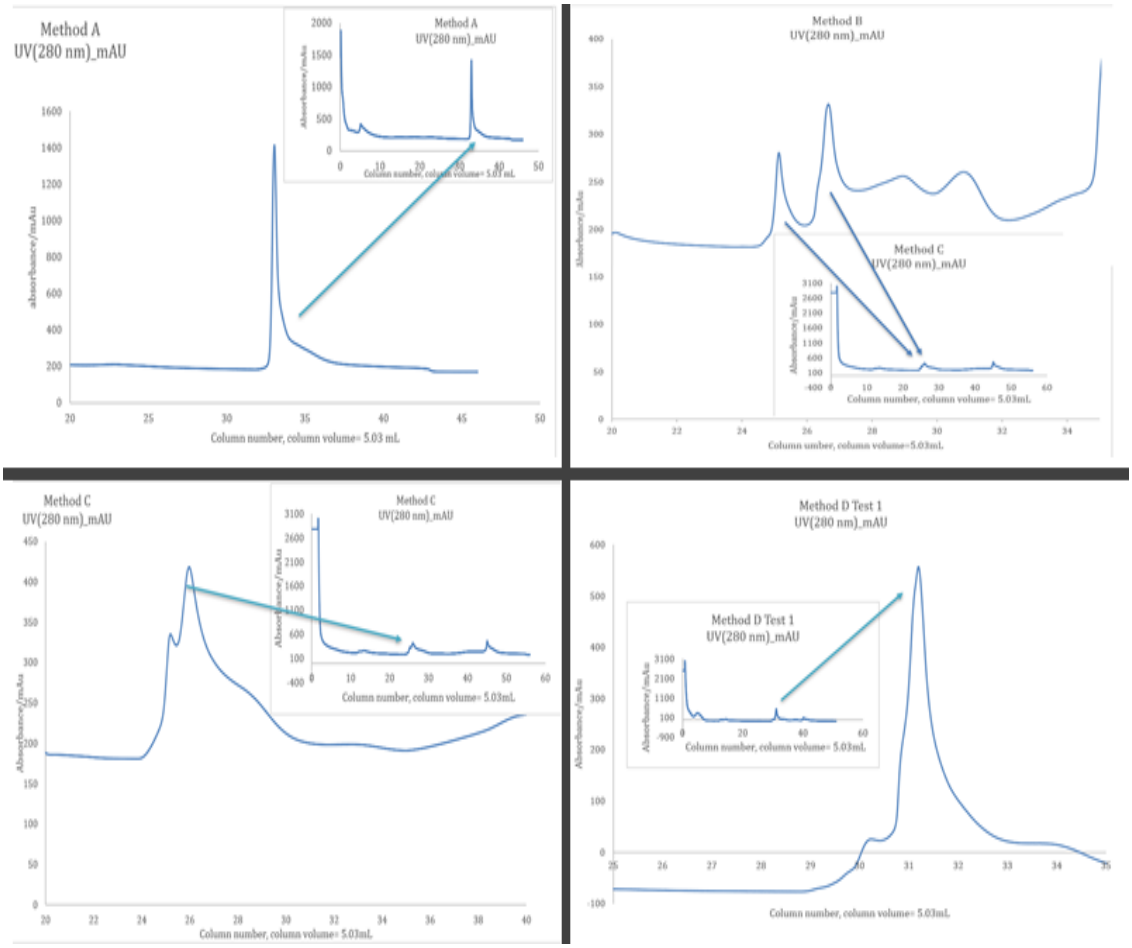

Figure 3.4: FPLC chromatogram of non-tagged DM constructed during IEX method A-D. Each graph shows one overall IEX and zoomed in where the protein is eluted.
A) In graph A protein eluted 228-252 mM NaCl (20-26 CV) and it was not on gradient. Another higher peak showed more color which was eluted at 600mM NaCl (33-36CV) at 100%B.
B) Protein eluted 330-360mM NaCl (28-32 CV).
C) Protein eluted in non-gradient 240-252 mM NaCl (25-35 CV)
D) Protein eluted in non-gradient 324-348mM NaCl (31-33 CV).

In all the different methods, method D showed to be a more effective method with better results. **Figure 3.5** shows 15% SDS-PAGE used to check purity of protein. We are expecting to see the 10.2 KDa band in to make sure this method is working.

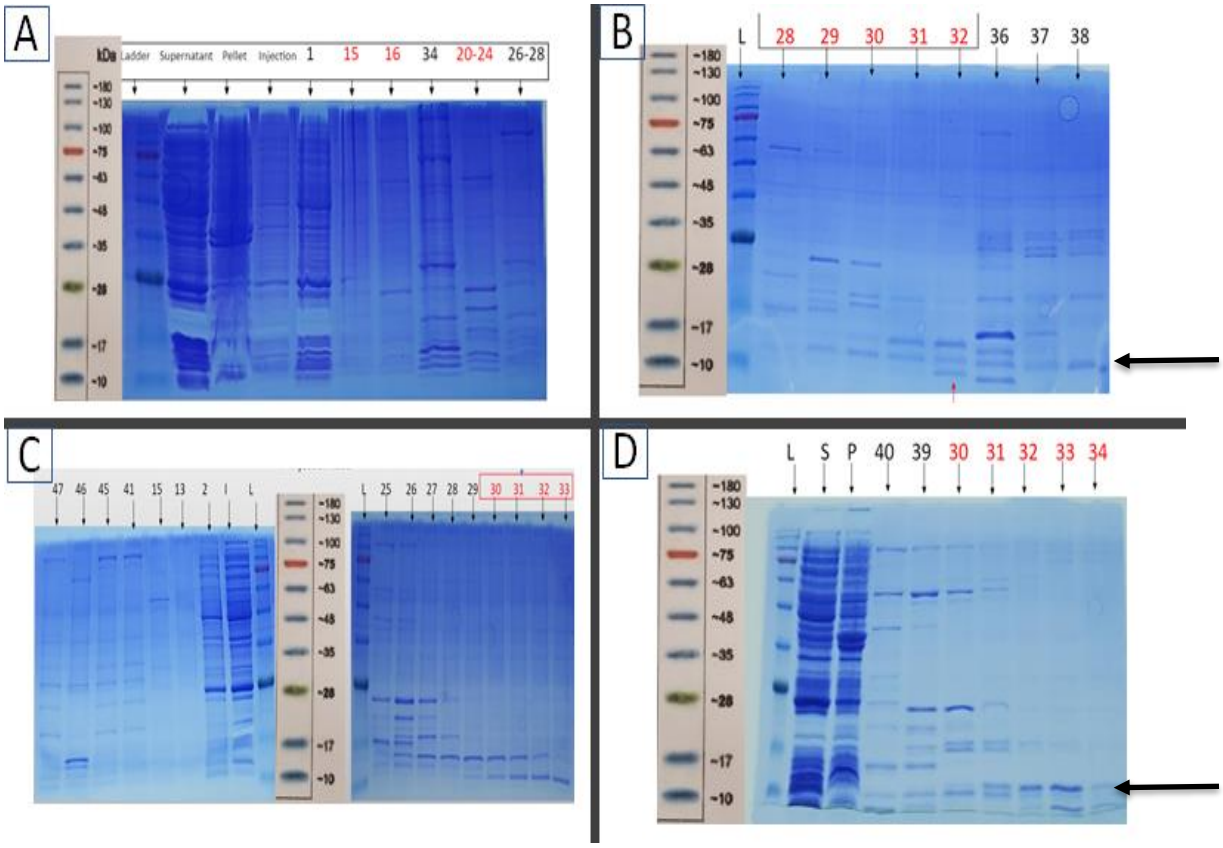

Figure 3.5: SDS-PAGE of DM non-tagged construct for method A-D: This is showing the 15% bis-acrylamide SDS-PAGE gel with non-tagged DM. The numbers on top refer to the column volume and red numbers refer to where red colors appeared, and protein expected to be ~ 10.2kDa**.**

- **A)** FPLC trace and gel shows that the protein eluted the early stage and non-gradient area which suggested that protein washed out of the column sooner than expected. The expected elution is 228-252mM NaCl and in a steep gradient. However, in this method the desired protein did not elute as expected (90mM NaCl) where pink color came out and it was not in gradient. Peaks that partially showed up in gradient 220-270mM NaCl showed no color.
- B) Light pink shows up around 330-360mM NaCl
- C) shows that the protein eluted in non-gradient areas and this suggest steepness of gradient is helping the protein elute in 240-252mM NaCl and so far, that method B still is the better option to purify our protein.
- D) Protein eluted on 324-348mM NaCl

Now that we made sure that method D is working on DM, we then further continued to purify protein with HiPrep 26/60 Sephacryl S-100 Size exclusion column and used SDS-PAGE to further confirm the purity of protein shows in **Figure 3.6** and **Figure 3.7.**

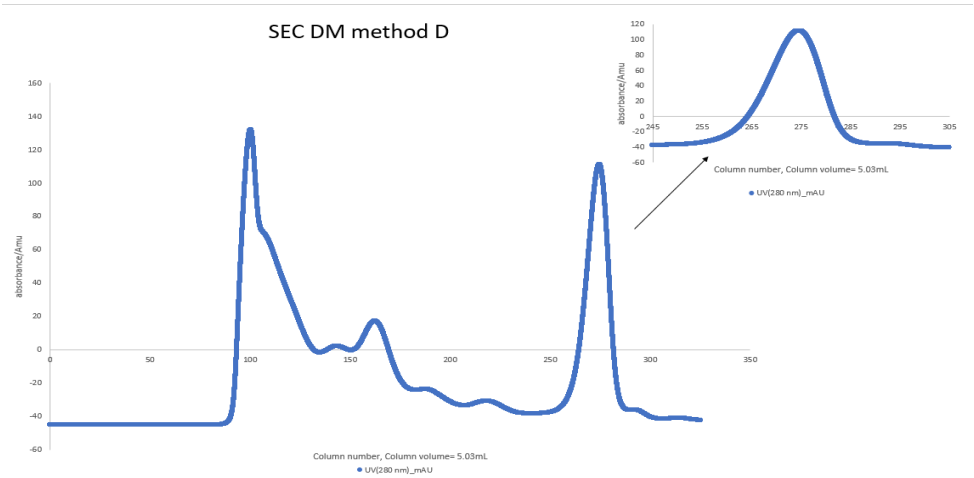

Figure 3.6: chromatogram of S 100 Size exclusion column purification step for DM non-tagged construct. Protein eluted 255-280 mL DM construct is separated fraction to test for content and purity of SDS-PAGE and which shown in **Figure 3.7.**

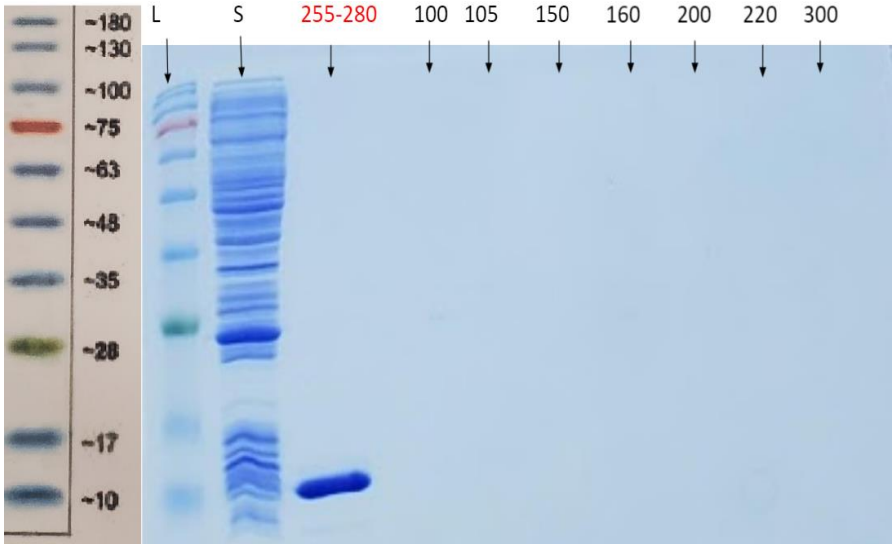

Figure 3.7: SDS-PAGE of SEC DM non-tagged construct for method D: This is showing the 15% bis-acrylamide SDS-PAGE gel with non-tagged DM. The numbers on top refer to the column volume and red numbers refer to where red colors appeared, and protein is expected to be ~ 10.2kDa**.** Protein eluted 255-280CV

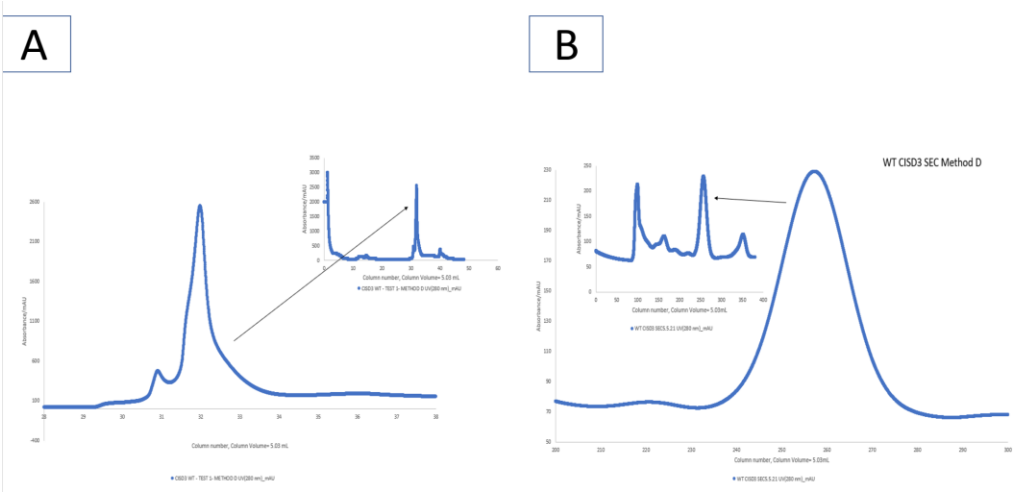

Figure 3.8: FPLC chromatogram of non-tagged WT (A) constructed during subsequent IEX, B) chromatogram of S 100 Size exclusion column purification step for WT non-tagged construct. Protein eluted IEX (A) (32-35 CV) and SEC (B) (240-280CV).

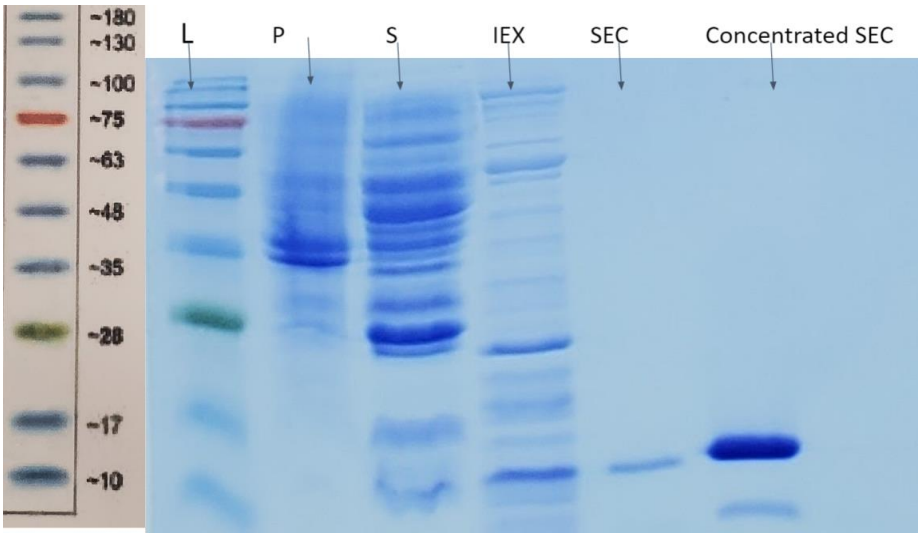

Figure 3.9: 15% SDS-PAGE ending with S100 column purification for non-tagged constructs.

In Conclusion, method D shows better results in purifying sensitive protein such as MiNT for both types of WT and mutant. Maintaining the stability of the protein on each step of purification is essential to obtain higher yield therefore reducing time of purification will result in a better yield since MiNT is very sensitive to temperature. Troubleshooting is ultimately needed in optimized yield for the protein purification. Purification shown above will serve as a foundation for further optimization, as the dynamics of MiNT become more elucidated.

Chapter 4

Characterization of human monomer NEET protein MiNT and stabilization by drug binding

Introduction

Human NEET proteins that contain CDGSH iron sulfur domains are as follows: mitoNEET (mNT, CISD1), nutrient-deprivation autophagy factor 1 (NAF-1, miner1, CISD2) and mitochondria inner NEET protein (MiNT, miner2, CISD3). Even though they have sequence differences, they are structurally homologous with a beta cap domain and cluster binding domain. MiNT is found in the mitochondrial matrix and plays a role in several human diseases, most significantly it is implicated in cancer.[11,56] NEET proteins are known to have redox sensor properties but specific biophysical characteristics of these proteins, specifically MiNT, is still poorly understood. According to the World Health Organization, almost 10 million people worldwide died of cancer in 2020, a number that is expected to rise to over 16 million annually by 2040.[57,58] Among the biggest problems facing current anticancer chemotherapeutics is chemotherapeutic resistance and lack of drug specificity, which leads to poor prognosis and severe toxicity.[59] As a result, novel approaches that are more potent and selective against cancer cells are required. The NEET class of proteins are a relatively new and unique class of [2Fe-2S]-containing proteins that are located on the outer mitochondrial membrane and endoplasmic reticulum (ER) of cells.[60] In known [2Fe-2S] proteins such as [2Fe-2S] ferredoxins,[61] the Fe-S clusters contain two iron metal centers that are each coordinated to two cysteine residues (**Figure 1A**). In NEET proteins, however, the [2Fe-2S] clusters are bound by two cysteine residues at one iron metal center and by a cysteine and a histidine residue at the other (**Figure 1B**). [33] The histidine ligand can render the iron-sulfur clusters labile, which causes the release of free iron.[45] In cancer

cells, certain levels of free iron have been shown to be beneficial for cellular proliferation.[62] Very high levels of free iron, however, can cause excessive reactive oxygen species (ROS) production, which can lead to irreparable cellular damage causing apoptosis and even ferroptosis.[63] Cancer cells therefore must tightly regulate the processes by which free iron and ROS are produced.[64] Recent studies on the role of NEET protein isoforms CISD1 (mitoNEET) and CISD2 (NAF-1) in breast cancer cells (Jennings & Theodorakis 2015) revealed that NEET proteins are highly involved in iron and ROS homeostasis and are also key contributors to cancer tumor growth and metastasis.[65] Disruption of NEETs could therefore offer a new therapeutic strategy against cancer whereby iron-overloaded cancer cells achieve a certain level of ROS-induced damage that leads to selective cancer cell death (**Figure 1D**). [36] Recently, the first class of small molecules in the caged xanthonoid class of natural products that selectively bind and destabilize NEET proteins have been identified. Binding of caged xanthonoid MAD28, for example, causes a destabilization of the wildtype NEET protein CISD1 [2Fe-2S] metal cluster, which in turn causes excessive release of free iron within cancer cells that eventually leads to cell death.[65]

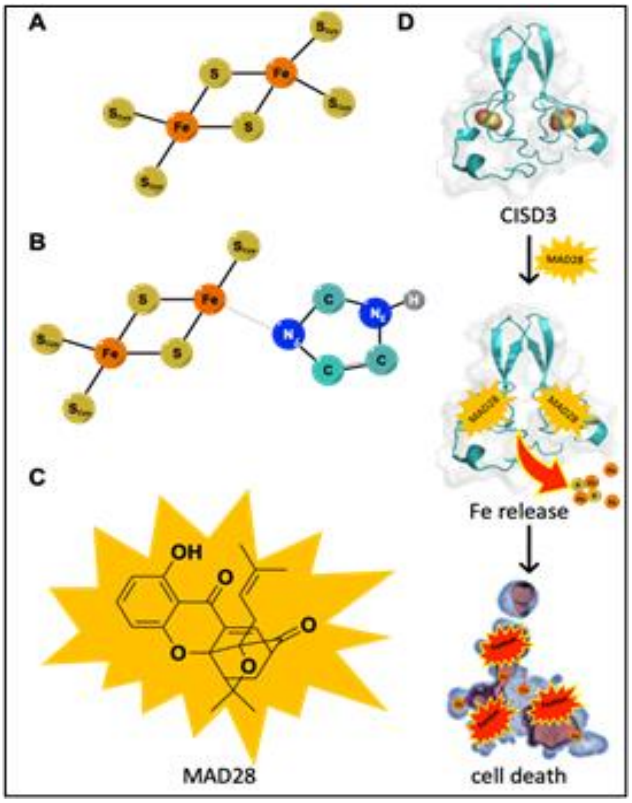

Figure 4.1. Schematic illustration that shows when MAD28 binds to CISD3 protein. A) Ligands of a typical [2Fe-2S] cluster. B) novel [2Fe-2S] cluster where a cysteine ligand has been replaced with histidine. C) Chemical structure of caged xanthone MAD28, a NEET destabilizer D) Proposed mechanism of NEET protein CISD1 destabilization by MAD28 leading to cell death. [33,36]

In this chapter we will highlight two different methods to analyze protein stability using two different drugs. Specifically, a UV-Vis spectroscopy assay and CD assay will detail changes to the overall protein stability upon drug binding. The stability of NEET protein binding for its [2Fe–2S] cluster was determined from monitoring their characteristic absorbance at 458 nm as a function of time. Previous studies have shown that the anti-diabetic drug pioglitazone was one of the first drugs described to interact with the CISD family of proteins. [66] To date, no studies have investigated potential ligand interaction of pioglitazone and DMSO with CISD3. Here we show that the thiazolidinediones

pioglitazone along with DMSO binds to CISD3. We hypothesize that MiNT (WT and mutant) will be stabilized by adding excess (~2 g/mL) Pioglitazone Hydrochloride (Pio) (Bosche Science) and 10% Dimethyl sulfoxide (DMSO). Furthermore, initial experiments with of MiNT with other caged xanthones will shed light on the general stability of the proteins. These preliminary findings may reveal additional pathways in the broader search for viable cancer treatments. Additionally, future aims in drug binding experiments with MiNT protein will be discussed in this chapter.

4.2 Method

4.2.1 Fe-S cluster transfer and stability assays in the presence of pioglitazone

Protein samples were generated for both WT and DM proteins in three conditions: (1) 20 μM in 50mM Tris–HCl pH 8.0, 150 mM NaCl buffer (2) similar conditions as (1) with 10% DMSO added, (3) similar conditions as (2) with excess (2 g/mL)Pio. Absorption spectra were recorded by UV-Vis from 200-800nm (CARY, 50Bio), with a temperature control apparatus set at 37 °C. Here, the focus of the absorbance changes was at 458 nm which is a signature [2Fe-2S] absorbance. Decays were performed at 37 °C and determined by monitoring loss of the 458 nm peak over time. Data were then fit to a single exponential **Figure 4.1** and **Figure 4.2.**

4.2.2 Stability assays using circular dichroism (CD) spectroscopy

Circular dichroism (CD) spectroscopy is a valuable biophysical tool for studying biomolecular protein structures.[67] Although CD does not provide residue specific information like Nuclear Magnetic Resonance (NMR) and X-ray crystallography, it has two major advantages. One advantage is that measurements are on small amounts of material which can be in physiological buffers. Another advantage is that it provides one of the best methods for monitoring any structural alterations that might result from changes in environmental conditions, such as pH, and temperature.[16] CD data is commonly reported as ellipticity, as it measures the differential absorbance of left and right circularly polarized light. The equation indicates the ellipticity relationship:

$$\text{Ellipticity} = \text{Theta} = 33.0\ (AL - AR)$$

Ellipticity (Theta) can be plotted against wavelength generating a typical CD spectrum**.** Ellipticities typically are in the range 10 mdeg. CD spectroscopy has proved to be an excellent tool for following protein-ligand interactions, mainly because of its ability to sensitively detect protein conformational changes. For this reason, it has emerged as an important tool for drug discovery, enabling screening for ligand interactions and drug binding.[16]

For the following experiments, we analyze MiNT (WT and mutant) protein in 50mM Tris–HCl pH 8.0, 150 mM NaCl buffer at a protein concentration of 20 µM. We then assessed similar protein samples with an addition of 10% DMSO, followed by protein samples with excess (2 g/mL) Pio. Individual spectra were recorded from 200-300nm with a temperature control apparatus. Multiple sets of wavelength scans were

collected at different temperatures:15°C,18°C and 37 °C, to assess the changes in stability of the proteins in the presence of Pio.

4.2.3 Fe-S cluster transfer and stability assay (UV-Vis) with gambogic acid

Using similar techniques in the assessment of Pio, additional experiments were conducted to assess cluster transfer and protein stability changes in the presence of gambogic acid. While the general experimental conditions were the same, the concentration of DMSO (1%) was changed to 10%DMSO. Experiments assessed the effects of both free gambogic acid (GA) and gambogic acid pyridine. After these two runs, we then used the same method to test GA01-130 derivative of GA but instead of 1% DMSO we used 10% DMSO to see any potential effects the increase DMSO would cause. Absorption spectra were recorded from 200-800nm (CARY, 50Bio), equipped with a temperature control apparatus set at 37 °C. Similar to previously described (4.2.2), changes in absorbance at 458 nm was observed over time.

Results and Discussion

The Crystal structure of MiNT (PDB ID no: 6AVJ) is the double mutant construct designed to help us to further understand WT MiNT. Stability assays using UV-Vis to monitor the change in absorbance at 458 nm were collected for both DM and WT in the presence of DMSO and Pio (**Figure 4.1** and **Figure 4.2.)**

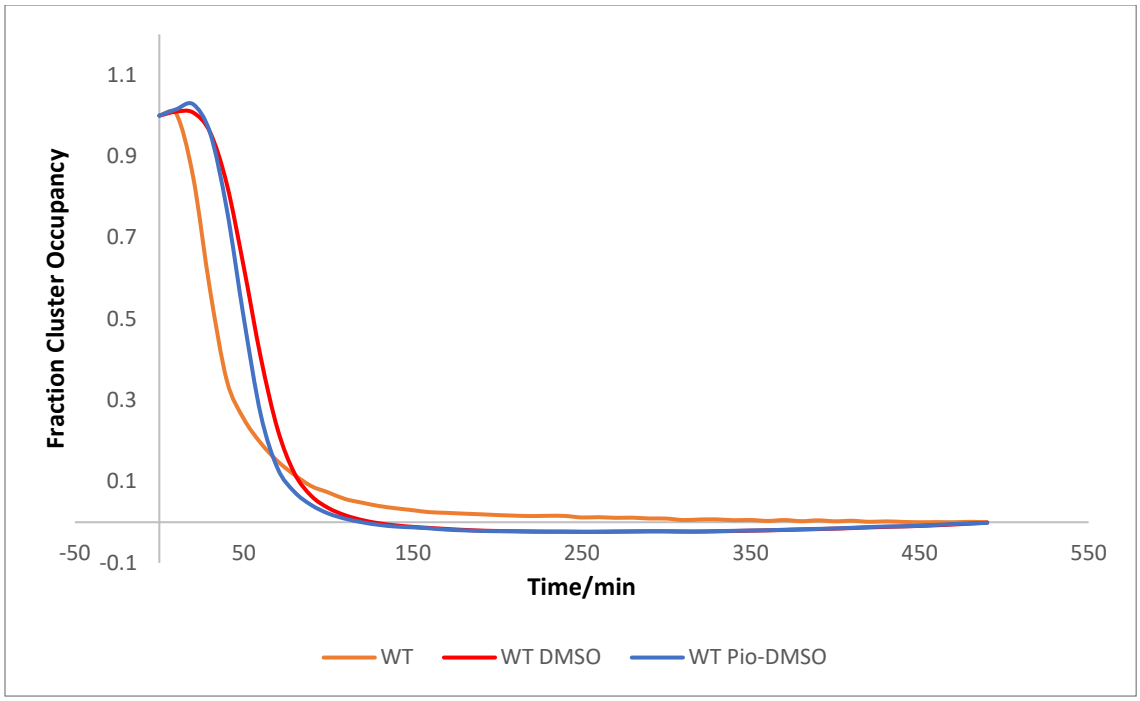

Figure 4.2: Decay and stability assay of the iron-sulfur clusters at 37 °C for WT with just Buffer, Buffer and 10% DMSO as well as pio 10% DMSO with buffer and 20µM purified protein. Buffer condition is Buffer conditions are 50mM Tris PH 8.0 and 150 mM NaCl. Orange line shows WT with buffer, Red line shows WT in buffer with 10%DMSO and Blue line shows WT in buffer with 10% pio DMSO.

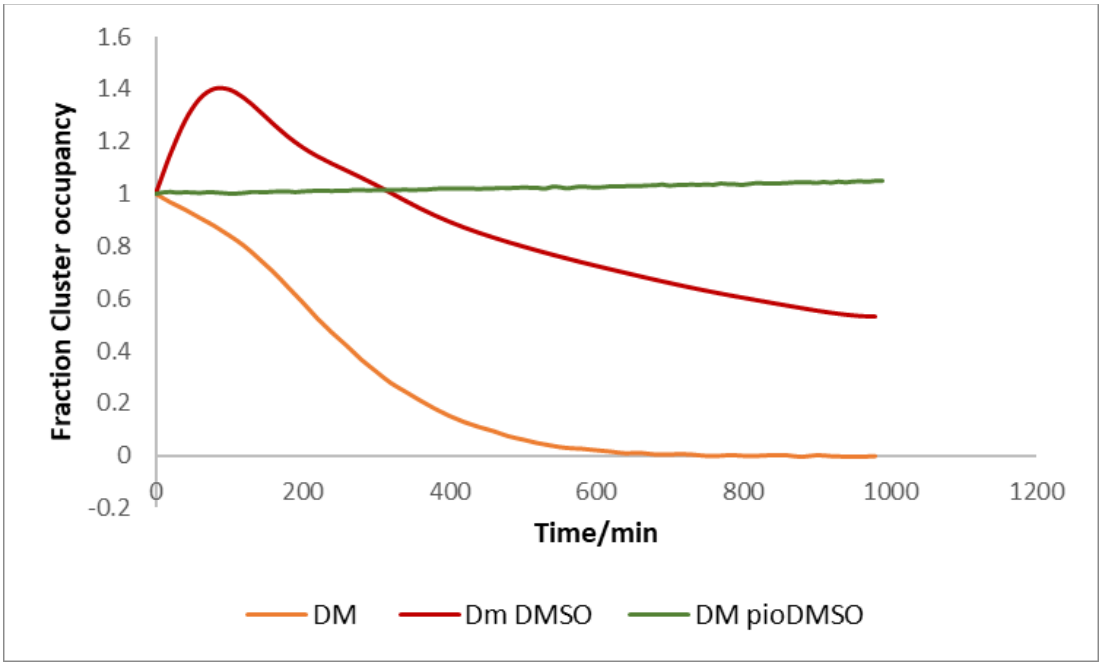

Figure 4.3: Decay and stability assay at 37 °C of the iron-sulfur cluster for Double- mutant MiNT. DM 20 µM with Buffer (Orange line) buffer contains 50mM Tris PH 8.0 and 150 mM NaCl, DM 10% DMSO (Red line) DM Pio DMSO (Green line), indicate a difference in the cluster stability over time.

Figure 4.2 and **figure 4.3** both indicate changes in protein stability in the presence of Pio-DMSO. While WT is not stable at high temperature, the initial data indicate that both Pio and DMSO increase the protein stability.

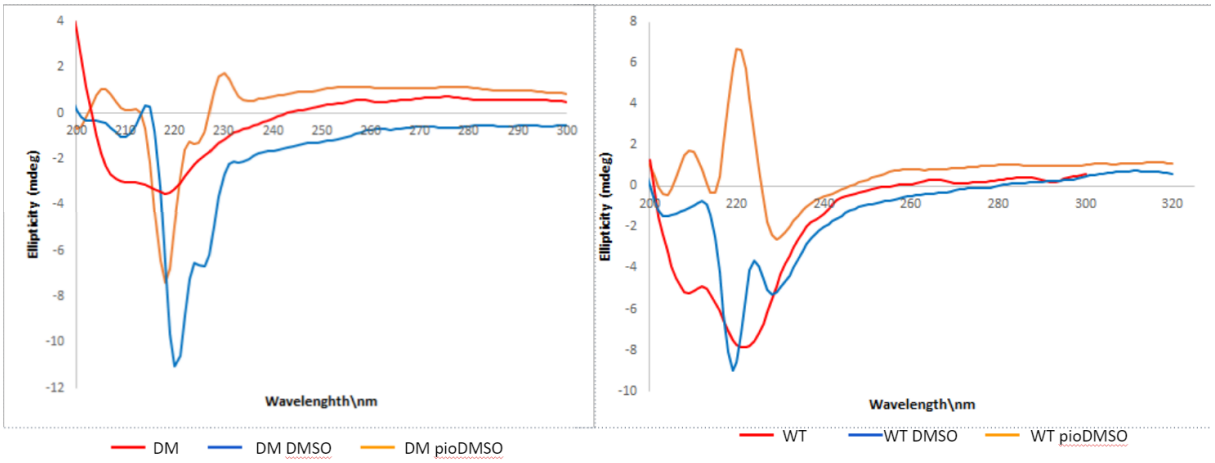

Figure 4.4 Circular dichroism spectra of 20μM MiNT and its mutant scanned in a range of 200 nm to 300 at 15°C. Different first run Just WT or DM with Buffer, Second WT or DM with 10% DMSO and lastly WT or DM with Pio 10% DMSO and 20μM purified protein. Buffer condition is Buffer SEC conditions are 50mM Tris PH 8.0 and 150 mM NaCl. Blue line shows WT/DM with/without DMSO, Orange line shows WT/DM with/without Pio and red line shows WT/DM with/without SEC buffer.

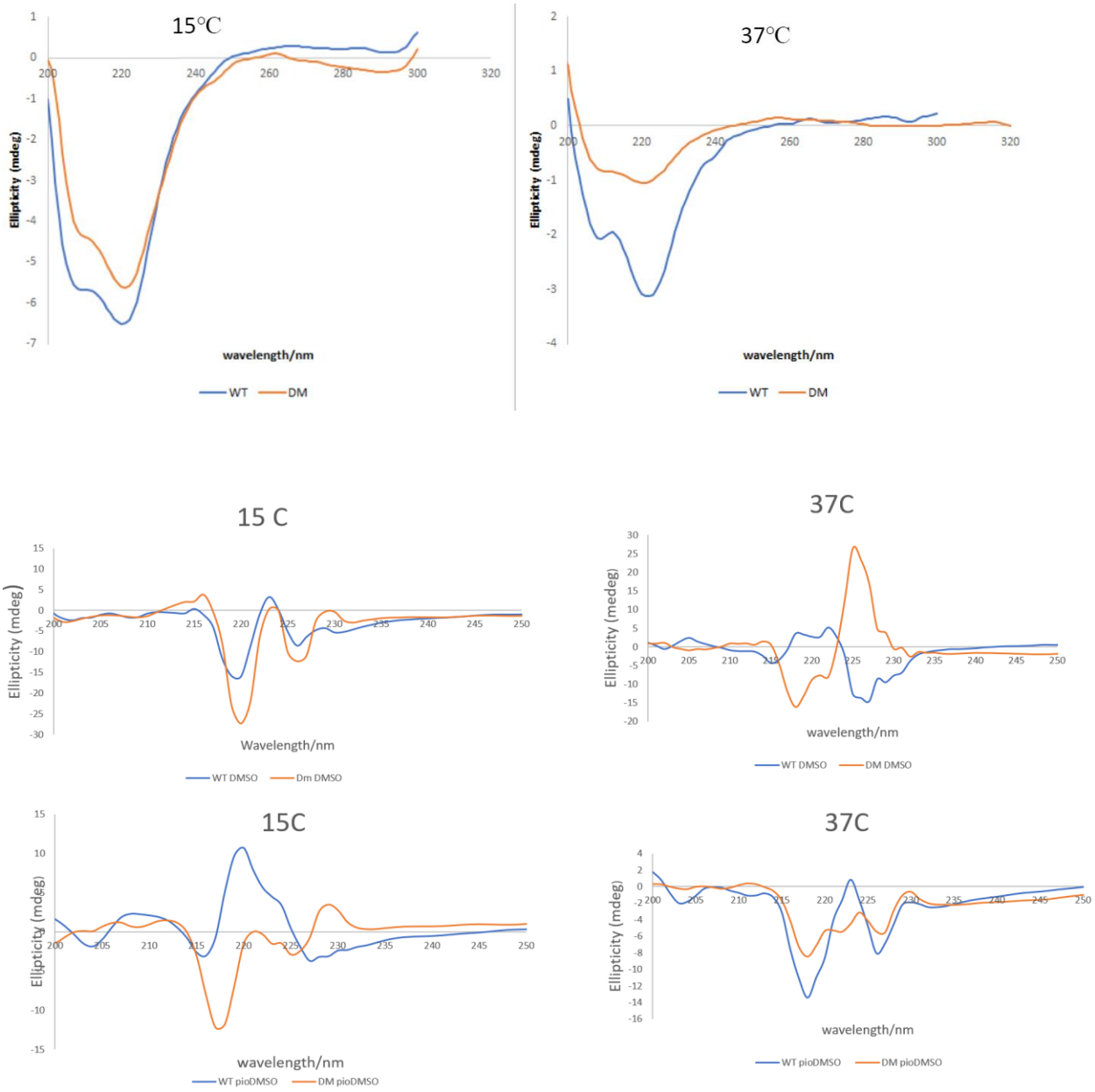

Figure 4.5 Circular dichroism spectra of 20μM MiNT an its mutant scanned in the range of 200 nm to 300 at both 15°C (left) and 37°C(right). The graphs indicate DM and WT with just buffer SEC, DM/WT with 10% DMSO and DM/WT with Pio and 10% DMSO at different temperatures. 20μM of protein (WT, blue; DM orange) in 50mM Tris pH 8.0 and 150 mM NaCl are presented in 15°C (left panels) and 37°C (right panels).

Figure 4.4 and **Figure 4.5** both indicate changes in protein conformation for DM and WT, at 15 and 37 °C, respectively, when adding Pio and DMSO. These preliminary results suggest that there are varations in the binding interactions for the respective conditions (Pio, DMSO, temperature) and further analysis is necessary in order to better understand the binding conformational dynamics. .

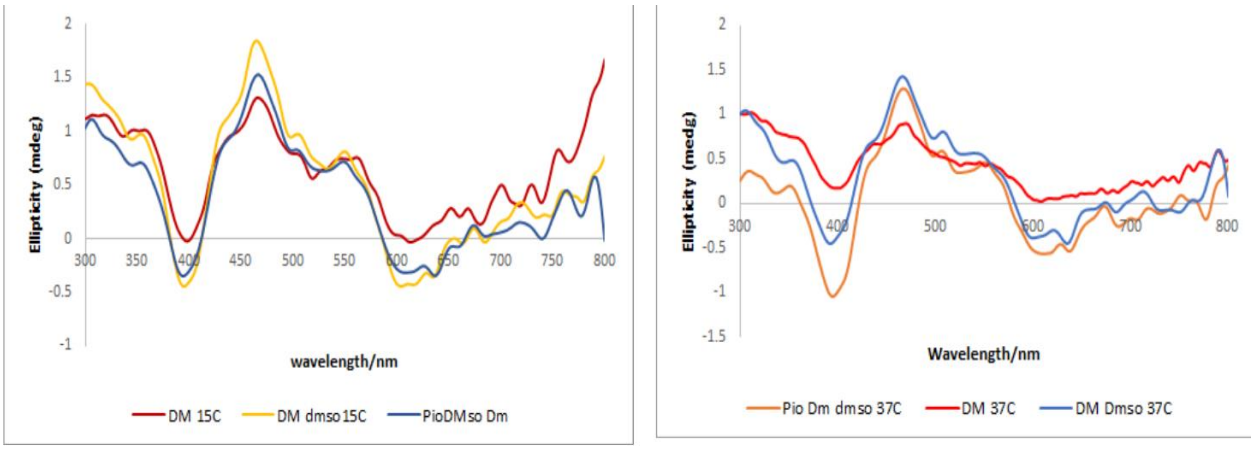

Figure 4.6: Circular dichroism spectra of DM 20μM MiNT and buffer, DM DMSO and DM pioDMSO in15 ℃ (right panel) 37℃ (left panel) . Buffer conditions in 50 mM Tris PH 8.0 and 150 mM NaCl. This figure indicates data collected from the CD to monitor the iron sulfur cluster in similar conditions as those monitoring the UV region of the spectra. While conformational changes were observed (**Figure 4.3** and **Figure 4.4),** these differences do not appear to relate to the iron-sulfur cluster interactions which prove the hypothesis that pio most likely binds to the side of the cluster away from cluster.

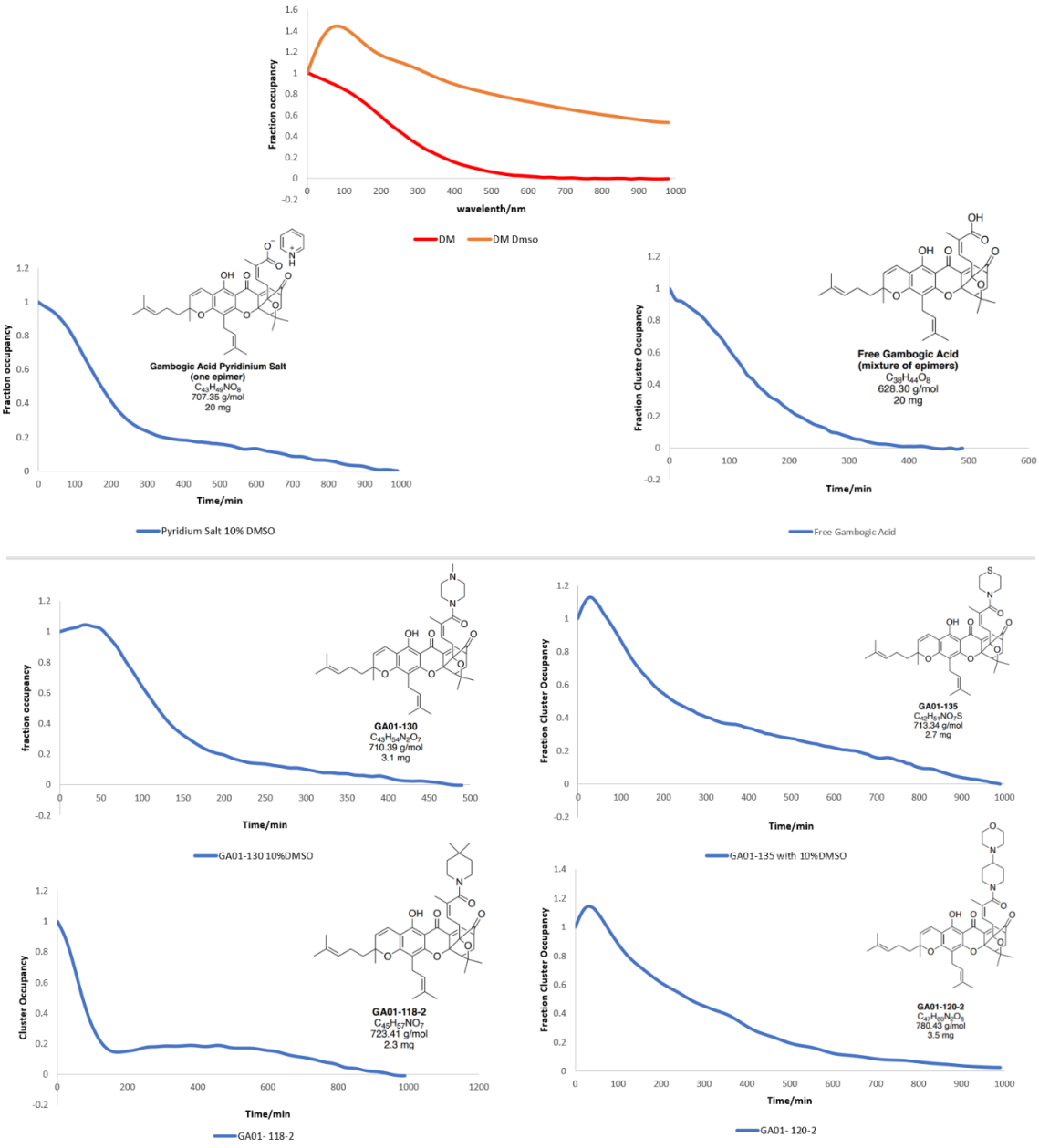

Figure 4.7: This figure shows Different derivatives of Gambogic Acid with DM CISD3. Blue line shows 50 µM of each derivative of Gambogic acid with 10% DMSO and 20 µM CISD3 DM protein and SEC buffer (SEC conditions are 50mM Tris PH 8.0 and 150 mM NaCl). Orange line shows protein with 10% DMSO which increases its stability. Red shows Protein with just an SEC buffer. X-axis shows wavelength in nm and y-axis shows fraction occupancy.

Since the preliminary data indicates conformational changes upon pio binding, we screened several gambogic acid analogs. Due to promising results obtained from our previous studies of the interaction between MAD28 and CISD1 and CISD2, the hypothesis is that caged xanthones analogs will also destabilize CISD3 which is another additional pathway in the search for a treatment of cancers. The half-life increased from ~320 min for just DM with buffer to ~600 min for DM with buffer and eventually stayed constant at 37 ℃ in DM with Pio- DMSO **Figure 4.3.** For WT, half-life increased from ~40min WT with buffer, 45 mins with DMSO and ~95 mins with Pio-DMSO **Figure 4.2** This show dependency on temperature for overall protein stability. Typical half-life of WT MiNT and WT NAF-1 is ~50 minutes and ~500 minutes, respectively.[68] while WT MiNT has a half-life of ~40 minutes.CD assay between 200 nm and 300 nm (**Figure 4.5**) might suggest that the WT MiNT construct might destabilize the Iron-sulfur cluster by changing its confirmation at 15° C which need further investigation and by that might reveal that WT with Pio and dmso have conformation change from negative to positive alpha helix. On the other hand**,** in this study **Figure 4.6** shows no conformational changes seen in the visible range of CD.

Concentrations of the MiNT constructs are usually calculated by using the 458 nm peak instead of the 280 nm peak as a single 2Fe-2S ligand extinction coefficient for NEET protein is about 10000 M^{-1} cm^{-1} using Arabidopsis NEET protein as a reference

Chapter 5

Mitochondrial Stress Response in Development and Regeneration of Muscle Fibers Once Exposed to Electronic Cigarettes: Electronic Cigarettes Vapor Deteriorates Mouse Skeletal Muscle Function Preventing Injury Recovery

5.1 Introduction

Cigarette smoking remains a leading cause of preventable disease and premature death in the United States and other countries.[69] On average, 435,000 people in the United States die prematurely from smoking-related diseases each year; overall, smoking causes 1 in 5 deaths. The chance that a lifelong smoker will die prematurely from a complication of smoking is approximately 50%. [70] Nicotine is the addictive molecule found in an important component of Electronic cigarettes (E-cigs), which acts as a mimic to the acetylcholine neurotransmitter that is involved in many functions including muscle movement, breathing and memory. Despite its potential noxious effects, nicotine intake is reinforced via the dopaminergic system [71-76] Within the nervous system, a synapse is a complex and specialized structure representing a junction point between two neurons shows in **Figure5.1**. A network of interconnected neurons forms a network of electrical activity where the synapse is the fundamental unit of electronic transfer. [72-73] Binding and release of neurotransmitters by neurons leads to a signal change inducing physiological changes to adjacent neurons. The neuromuscular junction (NMJ) is an example of a synapse formed between motor neurons and skeletal muscle fibers that is covered by Schwann cells (SCs).[74] NMJ formation requires intimate interactions among motor neurons, muscles, and SCs and is essential for controlling muscle contraction.[75] The ability of muscles to regenerate successfully depends on the following damage diminishes with age which appears to be a major contributor to the development of muscle weakness. [76]Muscle regeneration occurs early in the healing process where successful regeneration is dependent on

appropriate reinnervation of the injured muscle(s).[77] Although studies indicate that age may impact the interaction(s) between nerve and muscle, other external factors also contribute to slowed or impaired muscle repair. Significantly, constant exposure to nicotine may contribute to muscle weakness and physical frailty.[78-79] It is poorly understood how the use of E-cigs affects muscles and muscle recovery. More significantly, as E-cigs are targeted for young adults, understanding these effects will be vital in understanding recovery of muscles from injury and overall long-term health for this population **Figure 5.2**. The objective of this study is to test whether the exposure to E-cigs vapor weakens muscle function, limits exercise performance, or interferes with repair following injury. Here, inhalation of E-cig vapor delivers high doses of nicotine, raises systemic cytokine levels, and can compromise cardiopulmonary function. Through analysis of NMJ by changes in endplate size and pre- and post-apposition were observed suggesting changes in innervation. These initial data implicate E-Cig use as a negative impact on locomotive force development and exercise tolerance as a result of the compromised function of neuromuscular junctions.

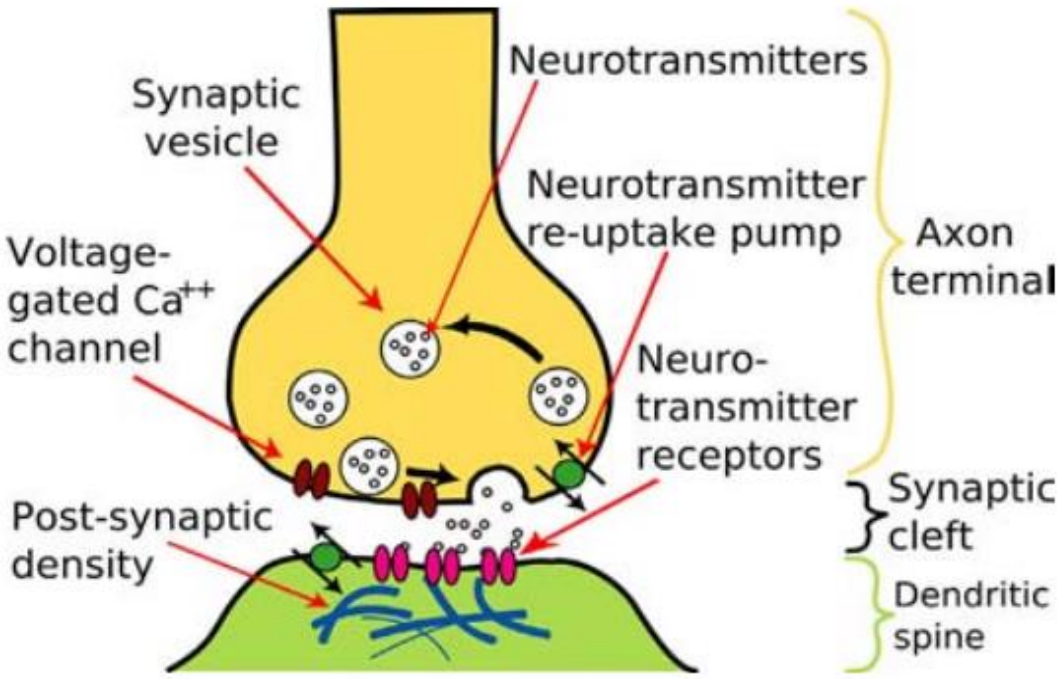

Figure 5.1: Chemical synaptic transmission. This graph is adopted from Kibenge paper and it shows Chemical synaptic transmission: chemical communication between an axon of a neuron and a dendrite of two separate neurons across a narrow extracellular space, the synaptic cleft. This is show how presynaptic and postsynaptic communicate and this is also shows that unconventional neurotransmitters like nitric oxide (NO) are not stored in synaptic vesicles and may carry messages from the postsynaptic neuron to the presynaptic neuron. Also, rather than interacting with receptors on the plasma membrane of their target cells, they can cross the cell membrane and act directly on molecules inside the cell. [80]

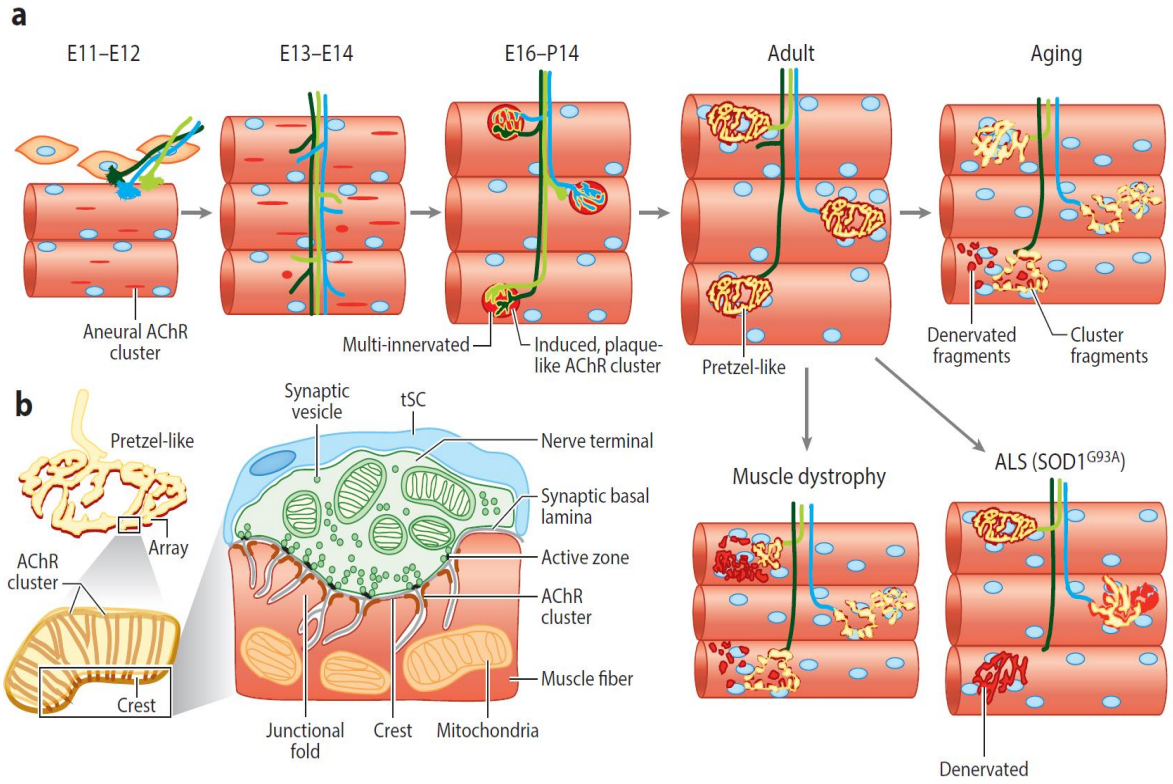

Figure 5.2: NMJ development in Mice at different ages. This figure is adopted from *Li. Xiong and Mei* paper. This shows NMJ development in mice at different ages and indicated contribution of mitochondria in muscle and nerve terminals. (a) Prior to the arrival of nerve terminals, myotubes form primitive, small, thin AChR clusters that are distributed in a broad middle region (axons E11–E12; E13–E14).Blue circles are nuclei shows inside muscle fibers and Red dashes indicated AChR cluster. Nerve-induced clusters are initially oval plaques, often innervated by multiple axons (E16–P14). As NMJs mature, AChR clusters become perforated and complex, resembling pretzels with arrays or branches that are innervated by one axon per NMJ (adult). AChR clusters become fragmented and denervated in aged mice and in muscular dystrophic mice.(b) NMJ structures at different magnifications.. [59]

5.2 Methods

Muscle mounting for NMJ analysis. Tibialis Anterior (TA) muscle from multiple mice were collected and placed inside a 2% paraformaldehyde-PBS solution overnight. These samples were collected from an injured and non-injured leg (right and left, respectively). After 24 hours, the muscles were placed in 1 mL of 30 % sucrose overnight to wash off excess paraformaldehyde. Subsequently, muscles were placed in 1mL 0.01% paraformaldehyde for storage in 4º C until the fiber separation step with the aid of the dissecting microscope. Fibers were subjected to a blocking buffer to ensure that the ACH receptor do not bind to any nonspecific antibodies during incubation which in 5% NGS, 5% BSA, 2% Triton X-100 in PBS for 24 hours. The muscle fibers were then incubated overnight with Alexa594-conjugated α-bungarotoxin (ThermoFisher Scientific, 5µg/mL concentration), a stable fluorescent dye used as a cell tracer that generates a signal for cell imaging, in order to identify acetylcholine receptors (AChR). Muscle bundles were mounted on slides with ProLong Gold Antifade Mountant (ThermoFisher Scientifics). After curing, slides were sealed with coverslips and magnets and stored in the dark 4º C until imaging. Additionally, the presynaptic motor neuron terminals are labeled with yellow fluorescent protein in (Thy1-YFP) mice.

Labeled neuron termini (Thy1-YFP and α-bungarotoxin) were detected by confocal microscopy with a Leica SP8 Confocal Lightening Deconvolution system using a 20X lens and 488 nm and 594 nm lasers, respectively. NMJ image stacks are collected with pre-established parameters using 400 dpi and various gains and Z-stacks for imaging. Maximal intensity projections were obtained using LASX software before analysis and calculation with Fiji. NMJ image stacks were collected with pre-established

parameters 400 dpi, 60%-80%gain, speed 500 Hz-700Hz, no offset, Z stack (500 – 1200 µm) all samples. Neuromuscular junctions were characterized for endplates based on total endplate area, pre and postsynaptic apposition between axon terminals, and AChRs. A total of ~ 640 samples of NMJs from all different groups having n=4 (n= number of mouse per group); AIR, VG/PG and E-CIGs groups were collected. As this initial study was conducted blind, all details regarding the mice and all the respective conditions (Air, E-Cigs, Injured, Non-injured, male/female) were withheld throughout the analyses.

5.3 Antibody Analysis

To check which antibody is suitable for the assay previously described to pinpoint the location of mitoNEET, testing of different secondary antibodies are required to check for cross-reactions. The first comparison is to check the differences between samples with and without a-bungarotoxin as mitoNEET is primarily located in the Outer Mitochondrial Membrane (OMM). And for positive control, keeping NMJ with YFP and bungarotoxin to show the NMJs can be detected. One of the mice right and left leg were incubating in α-bungarotoxin (Thermo Fisher scientific, 5ug/mL concentration) and fixed. The other mice right and left leg incubate in anti-mito-NEET, rabbit host for primary and secondary anti-rabbit with 633 nm. The result shows cross talk and photobleaching occurred therefore the result is unable to be determined as the excitation curve of 633 nm is interfering with the 594-excitation curve **Figure 5.3.**

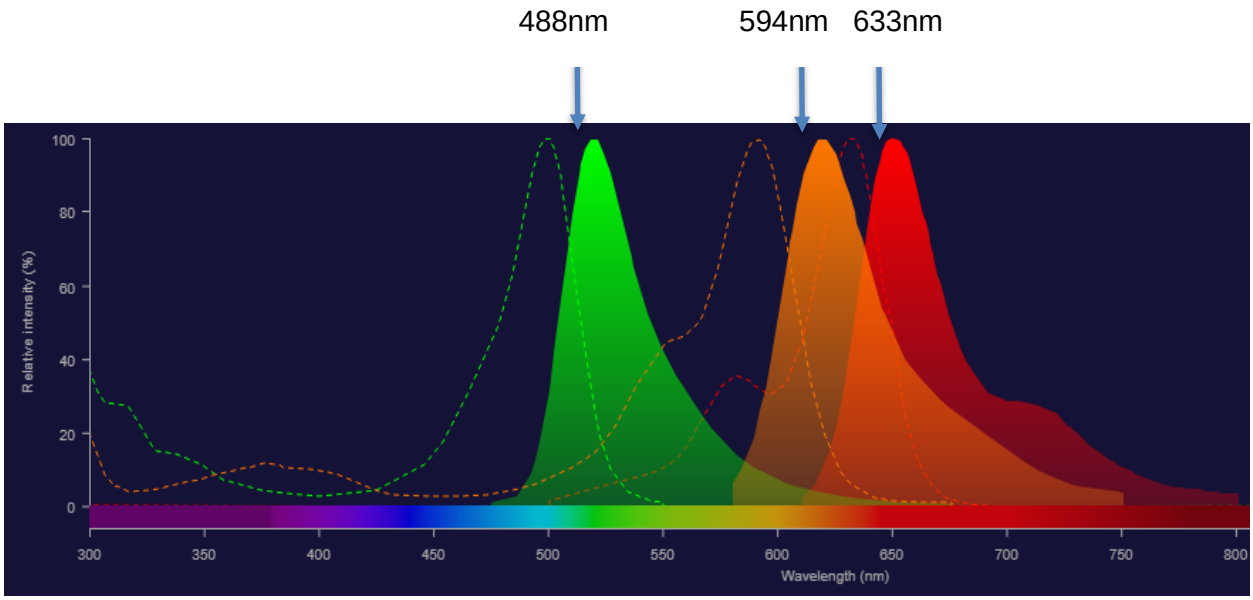

Figure 5.3: This is an emission and excitation curve. Alexa Fluor (Green,488 nm), Goat anti Mouse IgG (Orange,594 nm) and VDAC(Red,633nm) and it shows that 594 nm and 633 nm interfering.[81]

CISD1 with VDAC polyclonal antibody marker

Next, a similar assay was explored with a Mito-NEET Alexa Fluor 488 antibody. We use primary VDAC polyclonal antibody and secondary Alexa 546 Goat anti Mouse IgG (Thermo Fisher). After fiber incubation in a blocking buffer overnight, the fibers were washed with PBS and transfer to primary antibody CISD1 (1:200) (Thermo fisher) and subsequently transfer to secondary CISD1 antibody overnight. Then, transfer to primary VDAC antibody and next day transfer to secondary antibody Alexa Fluor 546 Goat anti-mouse IgG (1:400) (Thermo Fisher) **Figure 5.4.** The VDAC is used because we know that VDAC can be found at the mitochondria. In this experiment we wanted to find out the frequency of that in a normal NMJ, it was also to find the link between the CISDs and NMJ, and it requires further refinement.

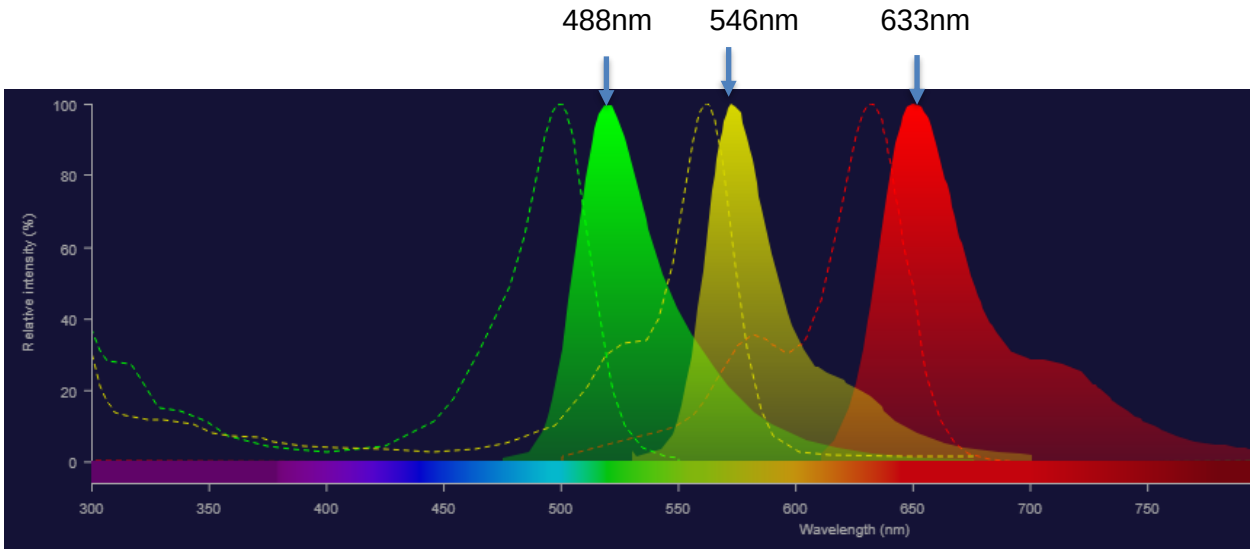

Figure 5.4 : This is an emission and excitation curve. Alexa Fluor (Green ,488 nm), α-bungarotoxin (Yellow,546 nm) and VDAC (Red,633nm) and it shows that 488 nm and 546 nm interfering more than 546 nm and 633nm.[46]

Alexa-594-α-bungarotoxin

In this assay, different mice were collected on both legs. This is to prove that bungarotoxin is marking the AChR. Figure1 shows that it usefully marks the α-bungarotoxin. In this assay after blocking with a buffer the next day, samples are washed with PBS and transfer to α-bungarotoxin (Thermo Fisher scientific, 5ug/mL concentration). Then seal and store in 4º C for one months until dried**. Figure 5.5** shows the α-bungarotoxin successfully marks the AChR (Red) and NMJs reveal a larger fragmented morphology.

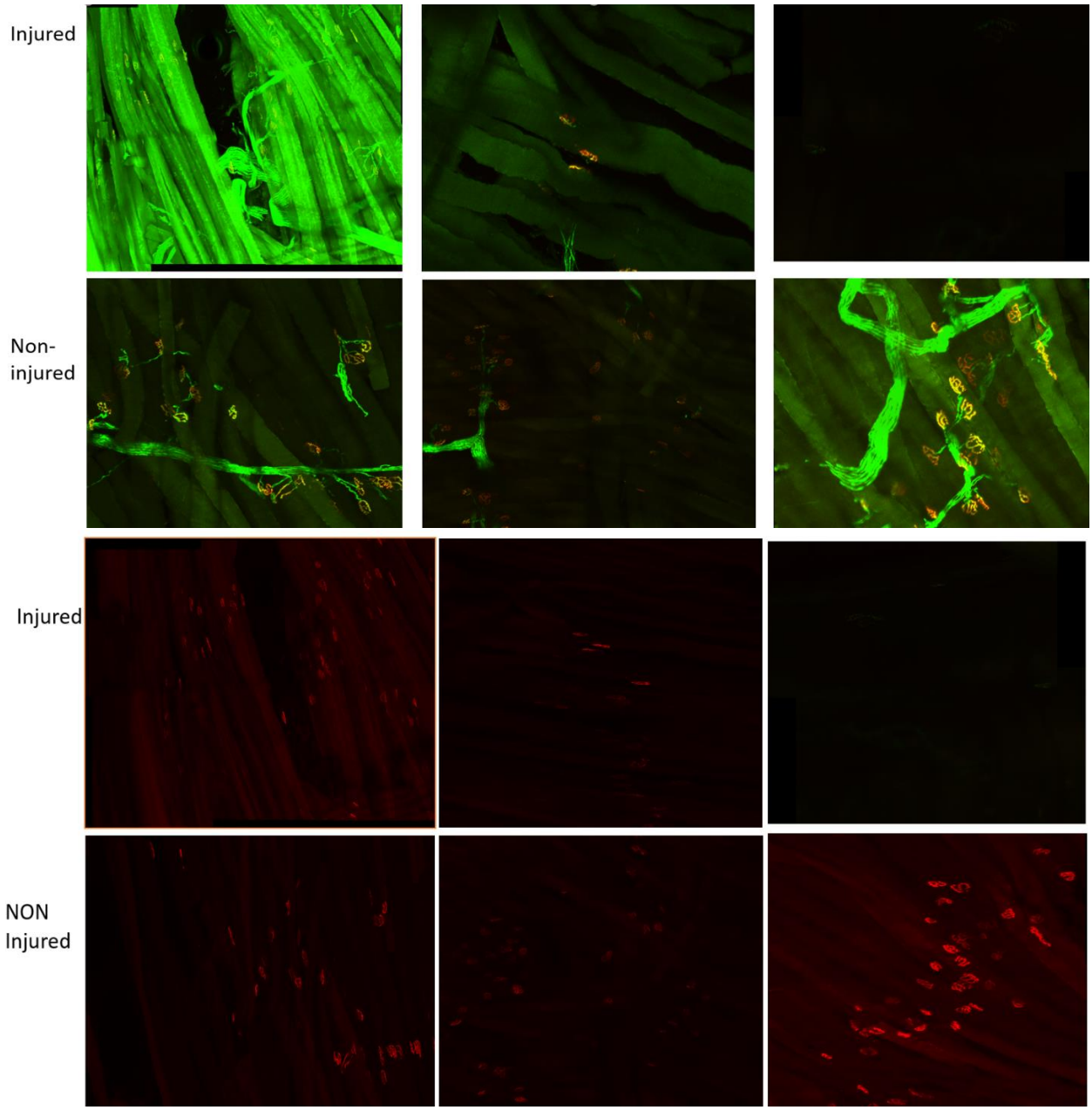

Figure 5.5: Representative NMJ images collected by confocal microscopy of each exposure group. Red - Alexa-594-α-bungarotoxin. Green – YFP labeled motor neurons. Bar = 20 µm. Yellow overlap of Red and Green . Figure 1A shows YFP+ Alexa-594-α-bungarotoxin. Figure 1B shows only Alexa-594-α-bungarotoxin. Representative images of NMJs in LCP-injured TA fiber bundles were captured at 20x (top) and (bottom). Green – YFP labeled motor neurons in Red – immunofluorescent detection of acetylcholine receptors with Alexa-594-α-bungarotoxin PG/VG+Nicotine NMJs reveal a larger, fragmented morphology. [82]

Alexa-594-α-bungarotoxin+Alexa-546-synaptophysin+YFP

In this experiment, after blocking muscles transferred to α-bungarotoxin overnight. Then the next day after PBS was washed, it was transferred to primary synaptophysin (1:200) for overnight incubation. Then the next day, transferred to secondary synaptophysin Alexa Fluor 546 (Thermo Fisher scientific, Goat Anti Rabbit IgG) (1:500). After three weeks of 4ºC storage, image them with confocal microscopy with a Leica SP8 Confocal Lightening Deconvolution system using a 20X lens and 488 nm, 594 nm, and 546 nm lasers **Figure 5.5**. As shown in **Figure 5.6** that is 546 nm and less interfering with YFP (488 nm) that already exists in muscles.

5.4 Results and discussion

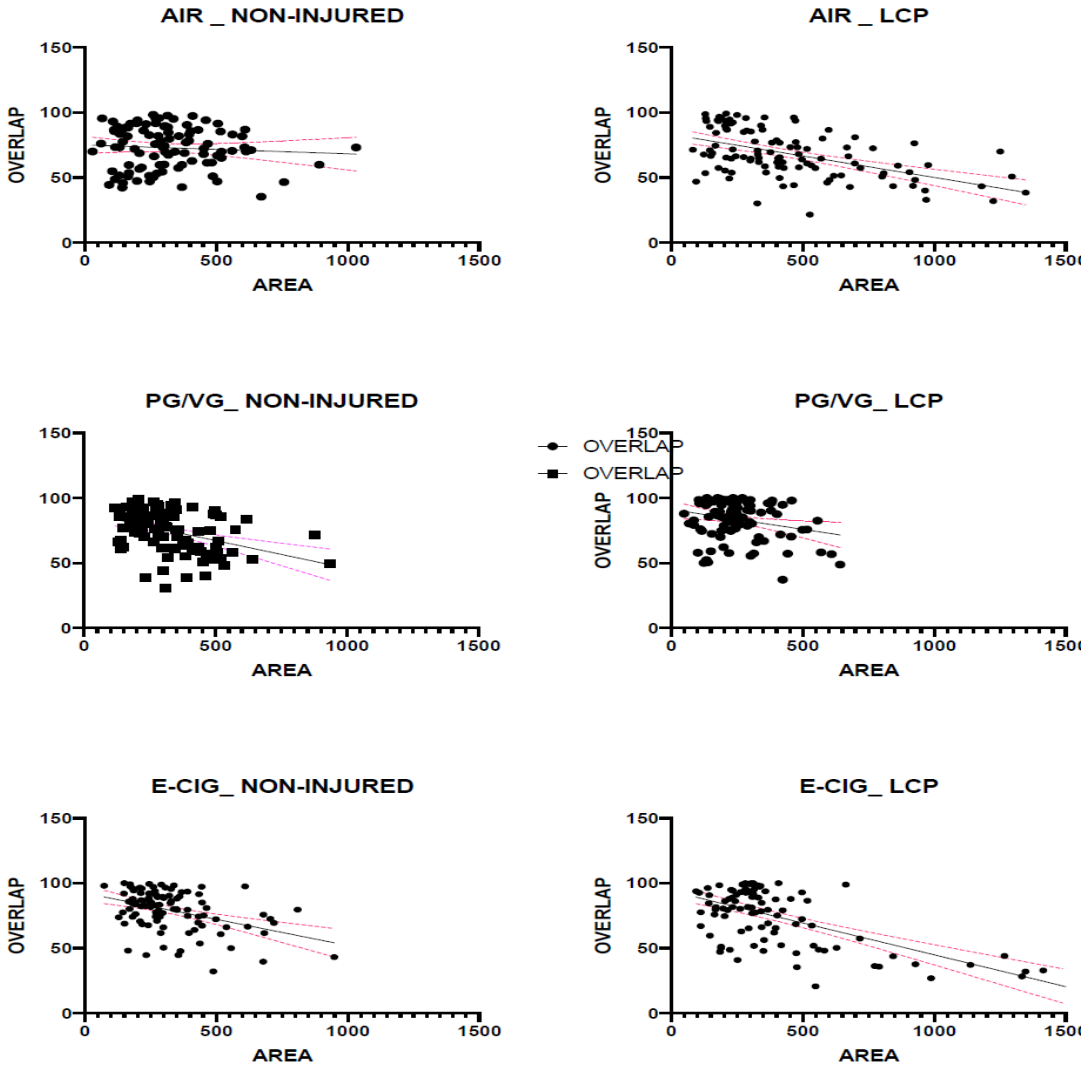

5.6 Correlation of pre- and post-synaptic apposition (%) and endplate area. highlight a sub-population of NMJs that are greater in size in the injured TA of the AIR and PG/VG+nicotine exposed groups. In contrast the NMJ in the TA of the PG/VG exposed mice reveal NMJ endplates with smaller more uniform areas and pre-/post-apposition percentages. Analysis of the percent pre- to post-apposition in large NMJs (> 500 um^2 endplate area) reveal a decrease in the injured TA compared to non-injured TA in the PG/VG+Nicotine exposed mice (p=0.026). Nicotine had a predominant effect on both metabolism and neuronal function mediated by catecholamines. The effects of PG/VG on muscle function are less clear but smaller NMJs with

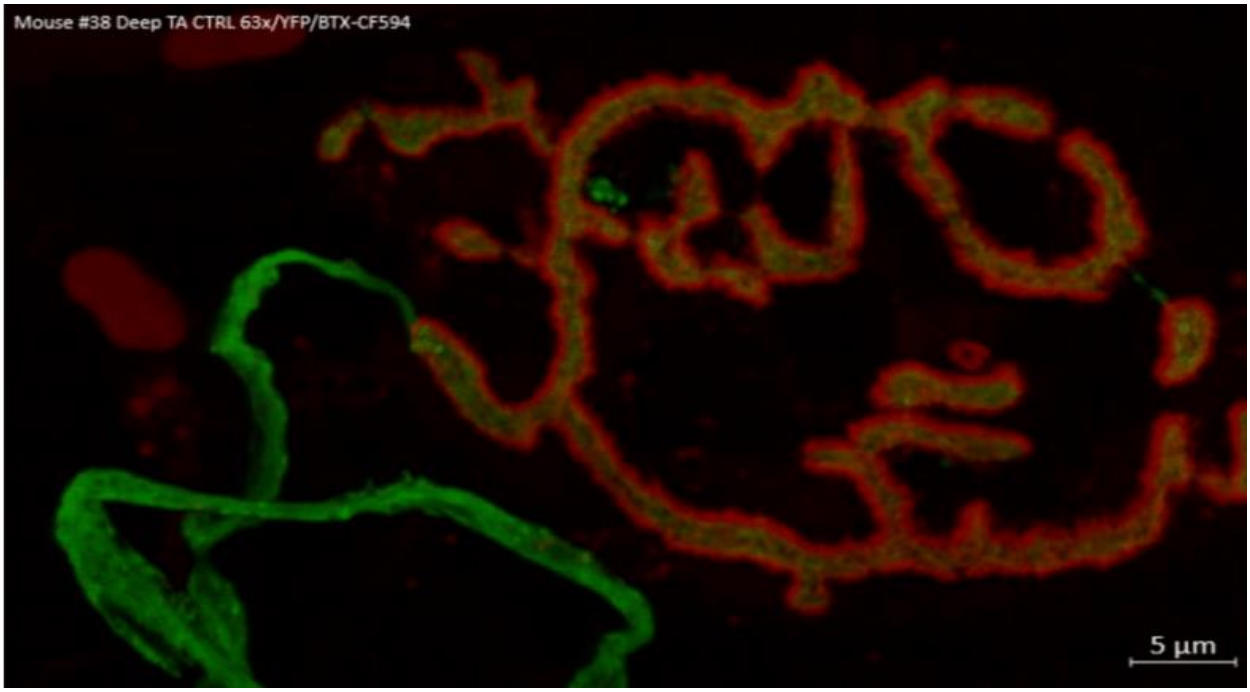

Figure 5.7 Maximum intensity projection (MIP) of Z-Stack through a neuromuscular junction (NMJ) in the deep region of the *Tibialis Anterior* (TA). Bundles of deep TA muscle fibers were treated with AF594-conjugated α-bungarotoxin to label nicotinic acetylcholine receptors in the neuromuscular junctions. YFP expressed in the axon and nerve terminal are green. Acetylcholine receptors are labeled in red, with areas of overlap appearing yellow. Markers of NMJ integrity, such as fragmentation, overlap, and area of synaptic contact can be evaluated from these images[82]

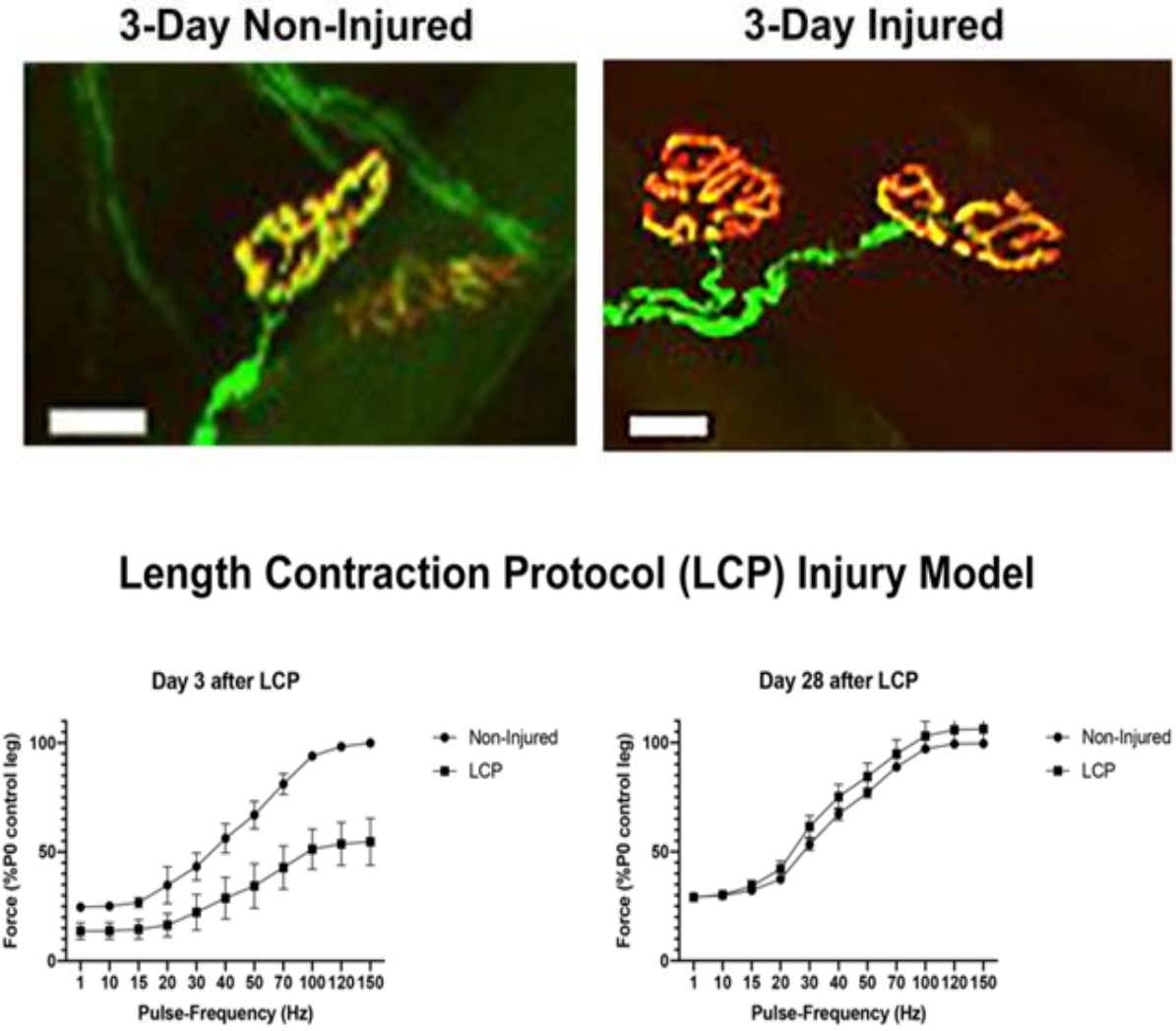

Figure 5.8 Muscle injury due to lengthening contractions (LCP).
(*TOP)* NMJs from the deep region of the TA showing overlap of neurons (YFP - green) and acetylcholine receptors (bungarotoxin - red). Non-complete overlap in injured muscle indicates partial innervation. Bar = 20 um*(Bottom)* At day 3 following the LCP, when NMJs and myofibers are disrupted, the force tested *ex-vivo* is decreased in the EDL and recovers by 28 days. [82]

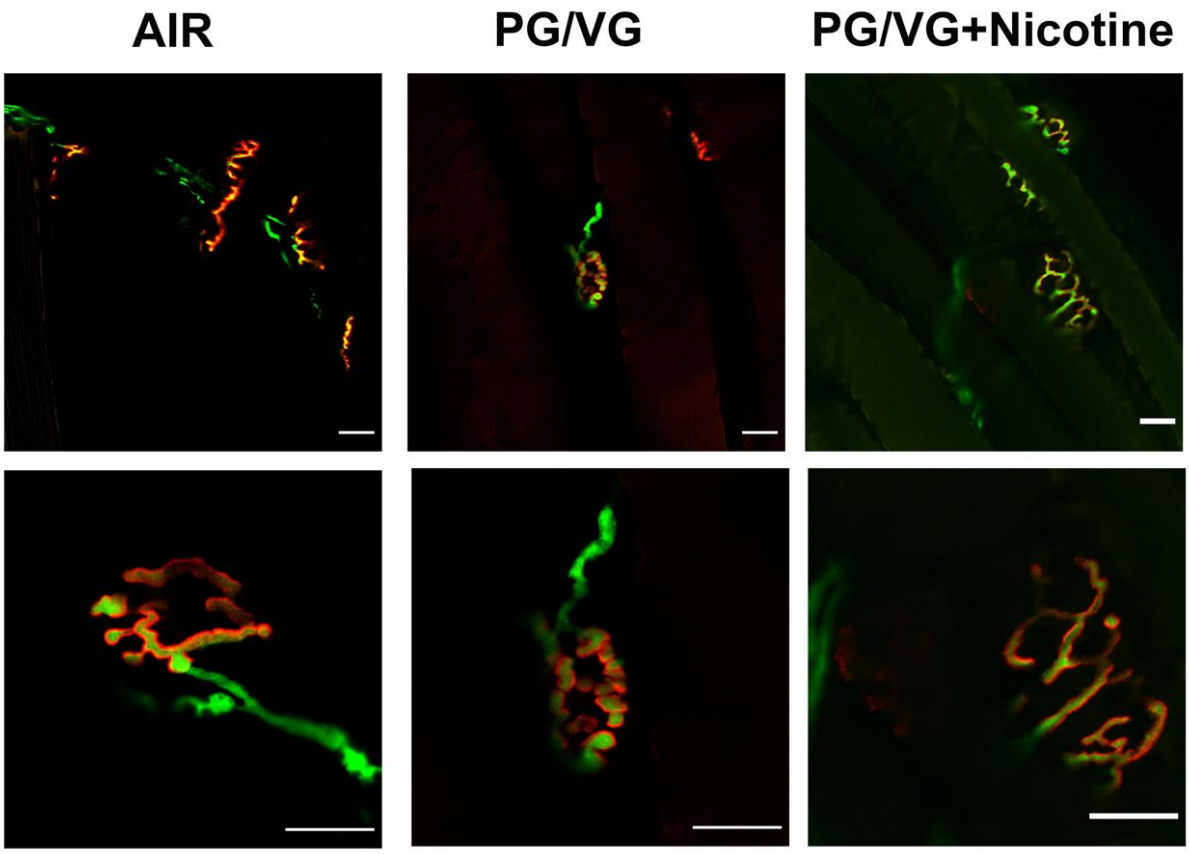

Figure 5.9: Representative NMJ images collected by confocal microscopy of each exposure group. Red - Alexa-594-α-bungarotoxin. Green – YFP labeled motor neurons. Bar = 20 µm. Representative images of NMJs in LCP-injured TA fiber bundles were captured at 20x (top) and 60x (bottom) magnification. Green – YFP labeled motor neurons in B6.Cg-Tg(Thy1-YFP)16Jrs/J mice. Red – immunofluorescent detection of acetylcholine receptors with Alexa-594-α-bungarotoxin. Bars = 20 µm. PG/VG+Nicotine NMJs reveal a larger, fragmented morphology [82]

Future Directions

Even though some characteristics of MiNT have been elucidated, further investigations have to be done to get a more accurate insight into the electron communication network of MiNT. Though MiNT has a role in several cancers, there are still many aspects of MiNT to be explored and the findings shown in this thesis will help illustrate further roles in the ISC pathways. Another significant thing about NEET is to further investigate NMJs in CISD protein to find out how CISD proteins contribute to sending signals from presynaptic to post synaptic vescles. A decline in mitochondrial function in skeletal muscle and white adipose tissue (WAT) is associated with aging and the progression of type 2 diabetes (T2D) and insulin resistance.[83,84,85,86] Accordingly, mitochondrial dysfunction is observed in the skeletal muscle of patients with type 2 diabetes and elderly people. [87,88]

Aim 1: Characterize the NEET binders via a combination of biochemical and biological assays. Working hypothesis is that NEET binders that destabilize the [2Fe-2S] cluster promote intracellular iron release, thereby altering iron metabolism and inducing cell death. Next step is to evaluate how potency and selectivity of the proposed NEET binders translates to cellular function. And then measure in vitro binding affinities of the synthesized molecules using established cluster stability and cluster transfer assays. Potent and paralog selective. NEET binders will be further characterized using cell-based assays in terms of mitochondrial localization and function (e.g., mitochondrial membrane depolarization, iron content and respiration) as well as cell death.

Aim2: Use Initial studies that performed in this thesis and further express NEET protein CISD3 and perform CISD3 binding studies of caged Garcinia xanthones library.

Aim 3: Further investigate CISD proteins' specifically CISD3 contribution on sending signal through neuromuscular junction and see how they contribute to muscles recovery.

References

1 William Gahl. National Human Genome Institute .https://www.genome.gov/genetics-glossary/Mitochondria (Accessed June 21,**2021**).

2 H. Reddy, P.; P. Reddy, T.. Mitochondria as a Therapeutic Target for Aging and Neurodegenerative Diseases. *Current Alzheimer Research* **2011**, *8* (4), 393–409.

3 Annesley SJ, Fisher PR. Mitochondria in Health and Disease. Cells. **2019** Jul 5;8(7):680. doi: 10.3390/cells8070680. PMID: 31284394; PMCID: PMC6678092.

4 Picard M, Taivassalo T, Gouspillou G, Hepple RT. Mitochondria: isolation, structure, and function. J Physiol. **2011** Sep 15;589(Pt 18):4413-21. doi: 10.1113/jphysiol.2011.212712. Epub 2011 Jun 27. PMID: 21708903; PMCID: PMC3208215.

5 Wallace DC. Mitochondrial disease in man and mouse.Science.**1999**;283:1482-1488

6 Chicco AJ, Sparagna GC. Role of cardiolipin alterations in mitochondrial dysfunction and disease. Am J Physiol Cell Physiol **2007**; 292:C33-C44.

7 Karbowski, M.; Neutzner, A.. Neurodegeneration as a consequence of failed mitochondrial maintenance. Acta Neuropathologica **2012**, 123 (2), 157–171.

8 Swerdlow RH. Brain aging, Alzheimer's disease and mitochondria. Biochim Biophys Acta **2011**; 1812(12):1630-1639.

9 Victor VM, Apostolova N, Herance R, Hernandez-Mijares A, Rocha M. Oxidative stress and mitochondrial dysfunction in atherosclerosis: mitochondria-targeted antioxidants as potential therapy. Curr Med Chem. **2009**;16(35):

10 Limongelli G, Masarone D, D'Alessandro R, Elliott PM. Mitochondrial diseases and the heart: an overview of molecular basis, diagnosis, treatment and clinical course. Future Cardiol. **2012** Jan;8(1)

11 Ma, Z. A.; Zhao, Z.; Turk, J.. Mitochondrial Dysfunction andβ-Cell Failure in Type 2 Diabetes Mellitus. *Experimental Diabetes Research* **2012**, *2012*, 1–11.

12 Ghafourifar P, Mousavizadeh K, Parihar MS, Nazarewicz RR, Parihar A, Zenebe WJ. Mitochondria in multiple sclerosis. Front Biosci. **2008** Jan 1;13:3116-26. doi: 10.2741/2913. PMID: 17981781

13 Maiese, K.; Daniela Morhan, S.; Zhong Chong, Z.. Oxidative Stress Biology and Cell Injury During Type 1 and Type 2 Diabetes Mellitus. *Current Neurovascular Research* **2007**, *4* (1), 63–71

14 Rossignol, D. A.; Frye, R. E.. Mitochondrial dysfunction in autism spectrum disorders: a systematic review and meta-analysis. *Molecular Psychiatry* **2012**, *17* (3), 290–314.

15 Konradi, C.; Eaton, M.; Macdonald, M. L.; Walsh, J.; Benes, F. M.; Heckers, S.. Molecular Evidence for Mitochondrial Dysfunction in Bipolar Disorder. *Archives of General Psychiatry* **2004**, *61* (3), 300.

16 Chitkara DK, Nurko S, Shoffner JM, Buie T, Flores A. Abnormalities in gastrointestinal motility are associated with diseases of oxidative phosphorylation in children. Am J Gastroenterol. **2003** Apr;98(4):871-7

17 Myhill S, Booth NE, McLaren-Howard J. Chronic fatigue syndrome and mitochondrial dysfunction. Int J Clin Exp Med. **2009**;2(1):1-16. Epub 2009 Jan 15

18 Cordero MD, de Miguel M, Carmona-López I, Bonal P, Campa F, Moreno-Fernández AM. Oxidative stress and mitochondrial dysfunction in fibromyalgia. Neuro Endocrinol Lett. **2010**;31(2):169-73. PMID: 20424583

19 Breeding PC, Russell NC, Nicolson GL. Integrative model of chronically activated immune-hormonal pathways important in the generation of fibromyalgia. *Br J Med Pract.* **2012**;5(3):a524–a534

20 Sotgia, F.; Martinez-Outschoorn, U. E.; Lisanti, M. P.. Mitochondrial oxidative stress drives tumor progression and metastasis: should we use antioxidants as a key component of cancer treatment and prevention?. *BMC Medicine* **2011**, *9* (1), 62.

21 Nicolson, G. L.. Lipid replacement therapy: a nutraceutical approach for reducing cancer-associated fatigue and the adverse effects of cancer therapy while restoring mitochondrial function. *Cancer and Metastasis Reviews* **2010**, *29* (3), 543–552

22 Gabridge MG. Metabolic consequences of Mycoplasma pneumoniae infection. Isr J Med Sci. **1987** Jun;23(6):574-9. PMID: 3117731

23 Ashida, H.; Mimuro, H.; Ogawa, M.; Kobayashi, T.; Sanada, T.; Kim, M.; Sasakawa, C.. Cell death and infection: A double-edged sword for host and pathogen survival. *Journal of Cell Biology* **2011**, *195* (6), 931–942.

24 Kerr, D. S.. Treatment of mitochondrial electron transport chain disorders: A review of clinical trials over the past decade. *Molecular Genetics and Metabolism* **2010**, *99* (3), 246–255.

25 Braymer, J. J.; Freibert, S. A.; Rakwalska-Bange, M.; Lill, R.. Mechanistic concepts of iron-sulfur protein biogenesis in Biology. *Biochimica et Biophysica Acta (BBA) - Molecular Cell Research* **2021**, *1868* (1), 118863.

26 Wächtershäuser, G.. Groundworks for an evolutionary biochemistry: The iron-sulphur world. *Progress in Biophysics and Molecular Biology* **1992**, *58* (2), 85–201.
27 Johnson, D. C., Dean, D. R., Smith, A. D., & Johnson, M. K. Structure, function, and formation of biological iron-sulfur clusters. *Annual review of biochemistry*, **2005**. *74*, 247–281

28 Barras, F. Iron-Sulfur Proteins: Structure, Function and Biogenesis. *eLS***. 2017**, 1–9.

29 Qi, W.; Cowan, J. A.. Structural, mechanistic and coordination chemistry of relevance to the biosynthesis of iron–sulfur and related iron cofactors☆. *Coordination Chemistry Reviews* **2011**, *255* (7-8), 688–699.

30 Schilke, B.; Voisine, C.; Beinert, H.; Craig, E.. Evidence for a conserved system for iron metabolism in the mitochondria of Saccharomyces cerevisiae. *Proceedings of the National Academy of Sciences* **1999**, *96* (18), 10206–10211.

31 Urzica, E.; Pierik, A. J.; Mühlenhoff, U.; Lill, R.. Crucial Role of Conserved Cysteine Residues in the Assembly of Two Iron−Sulfur Clusters on the CIA Protein Nar1. *Biochemistry* **2009**, *48* (22), 4946–4958.

32 Sharma, A. K.; Pallesen, L. J.; Spang, R. J.; Walden, W. E.. Cytosolic Iron-Sulfur Cluster Assembly (CIA) System: Factors, Mechanism, and Relevance to Cellular Iron Regulation. *Journal of Biological Chemistry* **2010**, *285* (35), 26745–26751.

33 Wachnowsky, C.; Fidai, I.; Cowan, J. A.. Iron–sulfur cluster biosynthesis and trafficking – impact on human disease conditions. *Metallomics* **2018**, *10* (1), 9–29.

34 Abou-Sleiman, P. M.; Muqit, M. M. K.; Wood, N. W.. Expanding Insights of Mitochondrial Dysfunction in Parkinson's Disease. *Nature Reviews Neuroscience* **2006**, *7* (3), 207.

35 Johri, A.; Beal, M. F.. Mitochondrial Dysfunction in Neurodegenerative Diseases. *Journal of Pharmacology and Experimental Therapeutics* **2012**, *342* (3), 619.

36 Paddock, M. L.; Wiley, S. E.; Axelrod, H. L.; Cohen, A. E.; Roy, M.; Abresch, E. C.; Capraro, D.; Murphy, A. N.; Nechushtai, R.; Dixon, J. E; Jennings, P, A. MitoNEET is a uniquely folded 2Fe 2S outer mitochondrial membrane protein stabilized by pioglitazone. *Proceedings of the National Academy of Sciences* **2007**, *104* (36), 14342–14347.

37 Lipper, C. H.; Karmi, O.; Sohn, Y. S.; Darash-Yahana, M.; Lammert, H.; Song, L.; Liu, A.; Mittler, R.; Nechushtai, R.; Onuchic, J. N.; Jennings, P. A.Structure of the human monomeric NEET protein MiNT and its role in regulating iron and reactive oxygen species in cancer cells. *Proceedings of the National Academy of Sciences* **2018**, *115* (2), 272–277.

38 Stockl, K. M.; Le, L.; Zhang, S.; Harada, A. S. M.. Risk of acute myocardial infarction in patients treated with thiazolidinediones or other antidiabetic medications. Pharmacoepidemiology and Drug Safety **2009**, 18 (2), 166–174.

39 Chang, N. C.; Nguyen, M.; Bourdon, J.; Risse, P.-A.; Martin, J.; Danialou, G.; Rizzuto, R.; Petrof, B. J.; Shore, G. C.. Bcl-2-associated autophagy regulator Naf-1 required for maintenance of skeletal muscle. *Human Molecular Genetics* **2012**, *21* (10), 2277–2287.

40 Wiley, S. E.; Murphy, A. N.; Ross, S. A.; Van Der Geer, P.; Dixon, J. E.. MitoNEET is an iron-containing outer mitochondrial membrane protein that regulates oxidative capacity. *Proceedings of the National Academy of Sciences* **2007**, *104* (13), 5318–5323.

41 Wiley SE, Andreyev AY, Divakaruni AS, Karisch R, Perkins G, Wall EA, van der Geer P, Chen YF, Tsai TF, Simon MI, Neel BG, Dixon JE, Murphy AN (**2013**) EMBO Mol Med 5:904–918

42 Paddock ML, Wiley SE, Axelrod HL, Cohen AE, Roy M, Abresch EC, Capraro D, Murphy AN, Nechushtai R, Dixon JE, Jennings PA (2007) Proc Natl Acad Sci USA 104:14342–14347

43 Conlan AR, Axelrod HL, Cohen AE, Abresch EC, Zuris J, Yee D, Nechushtai R, Jennings PA, Paddock ML (2009) J Mol Biol 392:143–153

44 Amr S, Heisey C, Zhang M, Xia XJ, Shows KH, Ajlouni K, Pandya A, Satin LS, El-Shanti H, Shiang R (2007) Am J Hum Genet 81:673–683

45 Paddock ML, Wiley SE, Axelrod HL, Cohen AE, Roy M, Abresch EC, Capraro D, Murphy AN, Nechushtai R, Dixon JE, Jennings PA (2007) Proc Natl Acad Sci USA 104:14342–14347

46 Karmi, O.; Marjault, H.-B.; Pesce, L.; Carloni, P.; Onuchic, J. N.; Jennings, P. A.; Mittler, R.; Nechushtai, R.. The unique fold and lability of the [2Fe-2S] clusters of NEET proteins mediate their key functions in health and disease. *JBIC Journal of Biological Inorganic Chemistry* **2018**, *23* (4), 599–612.

47 Sengupta, S.; Nechushtai, R.; Jennings, P. A.; Onuchic, J. N.; Padilla, P. A.; Azad, R. K.; Mittler, R.. Phylogenetic analysis of the CDGSH iron-sulfur binding domain reveals its ancient origin. *Scientific Reports* **2018**, *8* (1).

48 Lal, N.; Willcox, C. R.; Beggs, A.; Taniere, P.; Shikotra, A.; Bradding, P.; Adams, R.; Fisher, D.; Middleton, G.; Tselepis, C.; Wilcox, B. E.. Endothelial Protein C Receptor Is Overexpressed in Colorectal Cancer as a Result of Amplification and Hypomethylation of Chromosome 20q. *The Journal of Pathology: Clinical Research* **2017**, *3* (3), 155.

49 Geldenhuys, W. J.; Leeper, T. C.; Carroll, R. T.. Mitoneet as a Novel Drug Target for Mitochondrial Dysfunction. *Drug Discovery Today* **2014**, *19* (10), 1601.

50 Dias, V.; Junn, E.; Mouradian, M. M.. The Role of Oxidative Stress in Parkinson's Disease. *Journal of Parkinson's Disease* **2013**, *3* (4), 461–491.

51 Pure Link Quick Plasmid Miniprep Kits-2014.igem.org. http://2014.igem.org/wiki/images/e/ed/BGU_purelink_quick-plasmid_qrc.pdf accessed June 5, 2021

52 Susanto,C.; investigation of a Human Monomeric NEET Protein MiNT: Structural Properties and Comparison to Homolous Human NEET Proteins, mNT and NAF-1. Scholarship.org/uc/item/6dj0h32h

53 Nechushtai, R.; Conlan, A. R.; Harir, Y.; Song, L.; Yogev, O.; Eisenberg-Domovich, Y.; Livnah, O.; Michaeli, D.; Rosen, R.; Ma, V.; Luo, Y.; Zuris, J. A.; Paddock, M. L.; Cabantchik, Z. I.; Jennings, P. A.; Mittler, R.. Characterization of Arabidopsis NEET Reveals an Ancient Role for NEET Proteins in Iron Metabolism. *The Plant Cell* **2012**, *24* (5), 2139–2154.

55 https://web.expasy.org/cgi-bin/protparam/protparam1?P0C7P0@noft@ Accessed July1, 2020.

56 Wiley, S. E.; Murphy, A. N.; Ross, S. A.; Van Der Geer, P.; Dixon, J. E.. MitoNEET is an iron-containing outer mitochondrial membrane protein that regulates oxidative capacity. *Proceedings of the National Academy of Sciences* **2007**, *104* (13), 5318–5323.

57 Ferlay, J.; Colombet, M.; Soerjomataram, I.; Mathers, C.; Parkin, D. M.; Pineros, M.; Znaor, A.; Bray, F., Estimating the global cancer incidence and mortality in 2018: GLOBOCAN sources and methods. *Int J Cancer* **2019,** *144* (8), 1941-1953.

58 Ferlay, J.; Ervik, M.; Lam, F.; Colombet, M.; Mery, L.; Piñeros, M.; Znaor, A.; Soerjomataram, I.; Bray, F. Global Cancer Observatory: Cancer Today. Lyon, France: International Agency for Research on Cancer. https://gco.iarc.fr/today (accessed 21 June 2021).

59 Bukowski, K.; Kciuk, M.; Kontek, R., Mechanisms of multidrug resistance in cancer chemotherapy. *Int J Mol Sci* **2020,** *21* (9), 3233.

60 Tamir, S.; Paddock, M. L.; Darash-Yahana-Baram, M.; Holt, S. H.; Sohn, Y. S.; Agranat, L.; Michaeli, D.; Stofleth, J. T.; Lipper, C. H.; Morcos, F.; Cabantchik, I. Z.; Onuchic, J. N.; Jennings, P. A.; Mittler, R.; Nechushtai, R., Structure-function analysis of NEET proteins uncovers their role as key regulators of iron and ROS homeostasis in health and disease. *Biochim Biophys Acta* **2015,** *1853* (6), 1294-1315.

61 Armengaud, J.; Sainz, G.; Jouanneau, Y.; Sieker, L. C., Crystallization and preliminary X-ray diffraction analysis of a [2Fe-2S] ferredoxin (FdVI) from *Rhodobacter capsulatus*. *Acta Crystallogr D Biol Crystallogr* **2001,** *57* (Pt 2), 301-303.

62 Galadari, S.; Rahman, A.; Pallichankandy, S.; Thayyullathil, F., Reactive oxygen species and cancer paradox: To promote or to suppress? Free Radic Biol Med 2017, 104, 144-164.

63 Torti, S. V.; Torti, F. M., Iron and Cancer: 2020 Vision. *Cancer Res* **2020,** *80* (24), 5435-5448

64 Liou, G. Y.; Storz, P., Reactive oxygen species in cancer. Free Radic Res 2010, 44 (5), 479-496.

65 Bai, F.; Morcos, F.; Sohn, Y. S.; Darash-Yahana, M.; Rezende, C. O.; Lipper, C. H.; Paddock, M. L.; Song, L.; Luo, Y.; Holt, S. H.; Tamir, S.; Theodorakis, E. A.; Jennings, P. A.; Onuchic, J. N.; Mittler, R.; Nechushtai, R., The Fe-S cluster-containing NEET proteins mitoNEET and NAF-1 as chemotherapeutic targets in breast cancer. *Proc Natl Acad Sci U S A* **2015,** *112* (12), 3698-3703.

66 Colca JR, McDonald WG, Waldon DJ, Leone JW, Lull JM, Bannow CA, Lund ET, Mathews WR. Identification of a novel mitochondrial protein ("mitoNEET") cross-linked specifically by a thiazolidinedione photoprobe. Am J Physiol Endocrinol Metab. 2004 Feb;286(2):E252-60.

67 Kelly, S. M.; Jess, T. J.; Price, N. C.. How to study proteins by circular dichroism. *Biochimica et Biophysica Acta (BBA) - Proteins and Proteomics* **2005**, *1751* (2), 119–139.

68 Conlan, A. R.; Axelrod, H. L.; Cohen, A. E.; Abresch, E. C.; Zuris, J.; Yee, D.; Nechushtai, R.; Jennings, P. A.; Paddock, M. L.. Crystal Structure of Miner1: The Redox-active 2Fe-2S Protein Causative in Wolfram Syndrome 2. *Journal of Molecular Biology* **2009**, *392* (1), 143–153.

69 Grant, R. A.; Cielen, N.; Maes, K.; Heulens, N.; Galli, G. L. J.; Janssens, W.; Gayan-Ramirez, G.; Degens, H.. The Effects of Smoking on Whisker Movements: A Quantitative Measure of Exploratory Behaviour in Rodents. *Behavioural Processes* **2016**, *128*, 17–23.

70 Doll R, Peto R, Boreham J, Sutherland I. Mortality in relation to smoking: 50 years' observations on male British doctors. *BMJ.* 2004;328:1519.

71 Grant, R. A.; Cielen, N.; Maes, K.; Heulens, N.; Galli, G. L. J.; Janssens, W.; Gayan-Ramirez, G.; Degens, H.. The effects of smoking on whisker movements: A quantitative measure of exploratory behaviour in rodents. *Behavioural Processes* **2016**, *128*, 17–23.

72 Benowitz, N. L.. Nicotine Addiction. *New England Journal of Medicine* **2010**, *362* (24), 2295–2303.

73 Lodish H., Berk A., Zipursky S.L., Matsudaira, P., Baltimore, D., Darnell, J . Molecular Cell Biology. 4th edition. New York: W. H. Freeman; **2000**. Section 21.1, Overview of Neuron Structure and Function.

74 Kummer TT, Misgeld T, Sanes JR. **2006**. Assembly of the postsynaptic membrane at the neuromuscular junction: paradigm lost. Curr. Opin. Neurobiol. 16:74–82

75 Li, L.; Xiong, W.-C.; Mei, L.. Neuromuscular Junction Formation, Aging, and Disorders. *Annual Review of Physiology* **2018**, *80* (1), 159–188.

76 Vasilaki A, Jackson MJ. Role of reactive oxygen species in the defective regeneration seen in aging muscle. Free Radical Biology & Medicine. **2013** ;65:317-323

77 Murphy, M.; Kardon, G.. Origin of Vertebrate Limb Muscle. In *Current Topics in Developmental Biology*; Current Topics in Developmental Biology, **2011**; pp 1–32.

78 Grant, R. A., Cielen, N., Maes, K., Heulens, N., Galli, G. L., Janssens, W., Gayan-Ramirez, G., & Degens, H. **2016**. The effects of smoking on whisker movements: A quantitative measure of exploratory behaviour in rodents. *Behavioural processes*, *128*, 17–23.

79 Hibbs RE, Zambon AC. Nicotine and Agents Acting at the Neuromuscular Junction and Autonomic Ganglia. In: Brunton LL, Hilal-Dandan R, Knollmann BC. eds. *Goodman & Gilman's: The Pharmacological Basis of Therapeutics, 13e*. McGraw-Hill; Accessed June 18, **2021**

80 Kibenge, F. S. B.; Strange, R. J.. Introduction to the anatomy and physiology of the major aquatic animal species in aquaculture; **2021**; pp 1–111.

81 Fluorescence spectraviewer. (n.d.). Retrieved April 05, **2021**, from https://www.thermofisher.com/us/en/home/life-science/cell-analysis/labeling-chemistry/fluorescence-spectraviewer.html#!/

82 UCSD Microscopy Core-NINDS NS047101

83 J. Hoeks, P. Schrauwen. Muscle mitochondria and insulin resistance: a human perspectiveTrends Endocrinol. Metabol., 23 (**2012**), pp. 444-450,

84 B.M. Baker, C.M. Haynes Mitochondrial protein quality control during biogenesis and aging Trends Biochem. Sci., 36 (**2011**), pp. 254-261,

85 Yokokawa, T.; Kido, K.; Suga, T.; Sase, K.; Isaka, T.; Hayashi, T.; Fujita, S.. Exercise Training Increases CISD Family Protein Expression in Murine Skeletal Muscle and White Adipose Tissue. *Biochemical and Biophysical Research Communications* **2018**, *506* (3), 571–577.

86 Kusminski, C. M.; Scherer, P. E.. Mitochondrial Dysfunction in White Adipose Tissue. *Trends in Endocrinology & Metabolism* **2012**, *23* (9), 435–443

87 Kelley, D. E.; He, J.; Menshikova, E. V.; Ritov, V. B.. Dysfunction of Mitochondria in Human Skeletal Muscle in Type 2 Diabetes. *Diabetes* **2002**, *51* (10), 2944–2950.

88 Short, K. R.; Bigelow, M. L.; Kahl, J.; Singh, R.; Coenen-Schimke, J.; Raghavakaimal, S.; Nair, K. S.. Decline in Skeletal Muscle Mitochondrial Function with Aging in Humans. *Proceedings of the National Academy of Sciences* **2005**, *102* (15), 5618–5623.